

AD-A111 043

ROCKWELL INTERNATIONAL THOUSAND OAKS CA SCIENCE CENTER F/8 7/4
LASER CANDIDATE REACTIONS OF O2F.(U)
JUL 80 R D COOMBE, R K HORNE F29601-78-C-0039

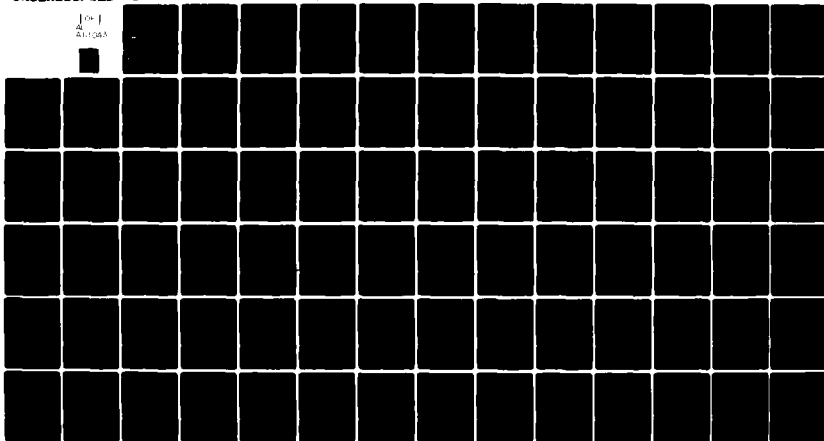
UNCLASSIFIED

SC5154.33FR

AFWL-TR-79-174

NL

TOP
ALL DATA



AFWL-TR-79-174

LEVEL

II

AFWL-TR-
79-174

2

AD A111043

LASER CANDIDATE REACTIONS OF O₂F

R. D. Coombe
R. K. Horne

Rockwell International Science Center
1049 Camino Dos Rios
Thousand Oaks, CA 91360

July 1980

Final Report

Approved for public release; distribution unlimited.

AIR FORCE WEAPONS LABORATORY
Air Force Systems Command
Kirtland Air Force Base, NM 87117

82 02 17025

DTIC FILE COPY



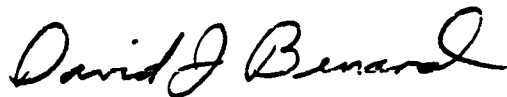
This final report was prepared by the Rockwell International Science Center, Thousand Oaks, California, under Contract F29601-78-C-0039, Job Order 33260310 with the Air Force Weapons Laboratory, Kirtland Air Force Base, New Mexico. Dr. David J. Benard (ARA) was the Laboratory Project Officer-in-Charge.

When US Government drawings, specifications, or other data are used for any purpose other than a definitely related Government procurement operation, the Government thereby incurs no responsibility nor any obligation whatsoever, and the fact that the Government may have formulated, furnished, or in any way supplied the said drawings, specifications, or other data, is not to be regarded by implication or otherwise, as in any manner licensing the holder or any other person or corporation, or conveying any rights or permission to manufacture, use, or sell any patented invention that may in any way be related thereto.

This report has been authored by a contractor of the United States Government. Accordingly, the United States Government retains a nonexclusive, royalty-free license to publish or reproduce the material contained herein, or allow others to do so, for the United States Government purposes.

This report has been reviewed by the Public Affairs Office and is releasable to the National Technical Information Service (NTIS). At NTIS, it will be available to the general public, including foreign nations.

This technical report has been reviewed and is approved for publication.

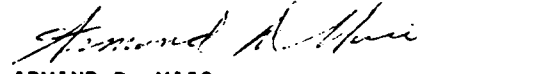


DAVID J. BENARD, PhD
Project Officer

FOR THE DIRECTOR



RONALD R. BOUSEK
Major, USAF
Chief, New Laser Concepts Br



ARMAND D. MAIO
Colonel, USAF
Chief, Advanced Laser Technology Div

DO NOT RETURN THIS COPY. RETAIN OR DESTROY

NOV 1979

UNCLASSIFIED

SECURITY CLASSIFICATION OF THIS PAGE (When Data Entered)

REPORT DOCUMENTATION PAGE		READ INSTRUCTIONS BEFORE COMPLETING FORM
1. REPORT NUMBER AFWL-TR-79-174	2. GOVT ACCESSION NO. AD A111043	3. RECIPIENT'S CATALOG NUMBER
4. TITLE (and Subtitle) LASER CANDIDATE REACTIONS OF O_2F	5. TYPE OF REPORT & PERIOD COVERED Final Report	
	6. PERFORMING ORG. REPORT NUMBER SC5154.33FR	
7. AUTHOR(s) R. D. Coombe, R. K. Horne	8. CONTRACT OR GRANT NUMBER(s) F29601-78-C-0039	
9. PERFORMING ORGANIZATION NAME AND ADDRESS Rockwell International Science Center 1049 Camino Dos Rios Thousand Oaks, CA 91360	10. PROGRAM ELEMENT, PROJECT, TASK AREA & WORK UNIT NUMBERS 61101F/33260310	
11. CONTROLLING OFFICE NAME AND ADDRESS Air Force Weapons Laboratory (ARA) Kirtland Air Force Base, NM 87117	12. REPORT DATE July 1980	
	13. NUMBER OF PAGES 80	
14. MONITORING AGENCY NAME & ADDRESS (if different from Controlling Office)	15. SECURITY CLASS. (of this report) Unclassified	
	15a. DECLASSIFICATION DOWNGRADING SCHEDULE	
16. DISTRIBUTION STATEMENT (of this Report) Approved for public release; distribution unlimited.		
17. DISTRIBUTION STATEMENT (of the abstract entered in Block 20, if different from Report)		
18. SUPPLEMENTARY NOTES		
19. KEY WORDS (Continue on reverse side if necessary and identify by block number)		
Dioxygen Monofluoride Magnesium Difluoride Metastables Dioxygenyl Fluoroarsenate Calcium Fluoride Photon Yields Halogen Monofluorides Chemical Reactions Lasers Magnesium Fluoride Chemiluminescence		
20. ABSTRACT (Continue on reverse side if necessary and identify by block number)		
<p>Gas phase O_2F radicals have been shown to be produced by the thermal decomposition of solid $O_2^+AsF_6^-$. O_2F generated in this manner exhibits a second order decay governed by a rate constant $k=1.4\pm0.4\times10^{11}$ cm³ mole⁻¹ sec⁻¹. Chemiluminescent reactions of O_2F with several added gases were observed. Electronically excited halogen monofluorides in the $A(^3\Pi_1)$ and $B(^3\Pi_0^+)$ states were produced by reactions of molecular halides with O_2F or by reactions of halogen atoms with O_2F in the presence of singlet molecular</p> <p style="text-align: right;">(over)</p>		

DD FORM 1 JAN 73 1473

UNCLASSIFIED

SECURITY CLASSIFICATION OF THIS PAGE (When Data Entered)

UNCLASSIFIED

SECURITY CLASSIFICATION OF THIS PAGE(When Data Entered)

20. ABSTRACT (Continued)

oxygen. The reactions of magnesium and calcium atoms with O_2F produced electronically excited MgF and CaF , respectively, in several accessible excited states. The measurement of photon yields for a number of these reactions indicated that direct production of excited electronic states is not a favored mechanism. On the contrary, the dominant mechanism in the reactions studied appears to be the production of vibrationally excited diatomic fluorides. The electronically excited species responsible for the visible-UV chemiluminescence are most likely formed either by resonant interactions with highly vibrationally excited ground state molecules or by collisional V-E energy transfer. ✓

UNCLASSIFIED

SECURITY CLASSIFICATION OF THIS PAGE(When Data Entered)

PREFACE

The work described herein is based upon earlier research performed by R.D. Coombe and Donald Pilipovich. Dr. Pilipovich, who left the Science Center prior to the beginning of this contract, shared in the origination of ideas concerning the generation of gaseous O_2F and its use as a chemical reagent. The authors are also grateful to Drs. A.T. Pritt, Jr., and F.J. Wodarczyk for numerous stimulating discussions during the course of this work.

Accession For	
PTIS 0001	<input checked="checked" type="checkbox"/>
PTIS 0002	<input type="checkbox"/>
PTIS 0003	<input type="checkbox"/>
PTIS 0004	<input type="checkbox"/>
PTIS 0005	<input type="checkbox"/>
PTIS 0006	<input type="checkbox"/>
PTIS 0007	<input type="checkbox"/>
PTIS 0008	<input type="checkbox"/>
PTIS 0009	<input type="checkbox"/>
PTIS 0010	<input type="checkbox"/>
PTIS 0011	<input type="checkbox"/>
PTIS 0012	<input type="checkbox"/>
PTIS 0013	<input type="checkbox"/>
PTIS 0014	<input type="checkbox"/>
PTIS 0015	<input type="checkbox"/>
PTIS 0016	<input type="checkbox"/>
PTIS 0017	<input type="checkbox"/>
PTIS 0018	<input type="checkbox"/>
PTIS 0019	<input type="checkbox"/>
PTIS 0020	<input type="checkbox"/>
PTIS 0021	<input type="checkbox"/>
PTIS 0022	<input type="checkbox"/>
PTIS 0023	<input type="checkbox"/>
PTIS 0024	<input type="checkbox"/>
PTIS 0025	<input type="checkbox"/>
PTIS 0026	<input type="checkbox"/>
PTIS 0027	<input type="checkbox"/>
PTIS 0028	<input type="checkbox"/>
PTIS 0029	<input type="checkbox"/>
PTIS 0030	<input type="checkbox"/>
PTIS 0031	<input type="checkbox"/>
PTIS 0032	<input type="checkbox"/>
PTIS 0033	<input type="checkbox"/>
PTIS 0034	<input type="checkbox"/>
PTIS 0035	<input type="checkbox"/>
PTIS 0036	<input type="checkbox"/>
PTIS 0037	<input type="checkbox"/>
PTIS 0038	<input type="checkbox"/>
PTIS 0039	<input type="checkbox"/>
PTIS 0040	<input type="checkbox"/>
PTIS 0041	<input type="checkbox"/>
PTIS 0042	<input type="checkbox"/>
PTIS 0043	<input type="checkbox"/>
PTIS 0044	<input type="checkbox"/>
PTIS 0045	<input type="checkbox"/>
PTIS 0046	<input type="checkbox"/>
PTIS 0047	<input type="checkbox"/>
PTIS 0048	<input type="checkbox"/>
PTIS 0049	<input type="checkbox"/>
PTIS 0050	<input type="checkbox"/>
PTIS 0051	<input type="checkbox"/>
PTIS 0052	<input type="checkbox"/>
PTIS 0053	<input type="checkbox"/>
PTIS 0054	<input type="checkbox"/>
PTIS 0055	<input type="checkbox"/>
PTIS 0056	<input type="checkbox"/>
PTIS 0057	<input type="checkbox"/>
PTIS 0058	<input type="checkbox"/>
PTIS 0059	<input type="checkbox"/>
PTIS 0060	<input type="checkbox"/>
PTIS 0061	<input type="checkbox"/>
PTIS 0062	<input type="checkbox"/>
PTIS 0063	<input type="checkbox"/>
PTIS 0064	<input type="checkbox"/>
PTIS 0065	<input type="checkbox"/>
PTIS 0066	<input type="checkbox"/>
PTIS 0067	<input type="checkbox"/>
PTIS 0068	<input type="checkbox"/>
PTIS 0069	<input type="checkbox"/>
PTIS 0070	<input type="checkbox"/>
PTIS 0071	<input type="checkbox"/>
PTIS 0072	<input type="checkbox"/>
PTIS 0073	<input type="checkbox"/>
PTIS 0074	<input type="checkbox"/>
PTIS 0075	<input type="checkbox"/>
PTIS 0076	<input type="checkbox"/>
PTIS 0077	<input type="checkbox"/>
PTIS 0078	<input type="checkbox"/>
PTIS 0079	<input type="checkbox"/>
PTIS 0080	<input type="checkbox"/>
PTIS 0081	<input type="checkbox"/>
PTIS 0082	<input type="checkbox"/>
PTIS 0083	<input type="checkbox"/>
PTIS 0084	<input type="checkbox"/>
PTIS 0085	<input type="checkbox"/>
PTIS 0086	<input type="checkbox"/>
PTIS 0087	<input type="checkbox"/>
PTIS 0088	<input type="checkbox"/>
PTIS 0089	<input type="checkbox"/>
PTIS 0090	<input type="checkbox"/>
PTIS 0091	<input type="checkbox"/>
PTIS 0092	<input type="checkbox"/>
PTIS 0093	<input type="checkbox"/>
PTIS 0094	<input type="checkbox"/>
PTIS 0095	<input type="checkbox"/>
PTIS 0096	<input type="checkbox"/>
PTIS 0097	<input type="checkbox"/>
PTIS 0098	<input type="checkbox"/>
PTIS 0099	<input type="checkbox"/>
PTIS 0100	<input type="checkbox"/>

DTIC
CROSS
INSPECT

A

TABLE OF CONTENTS

	Page
I. INTRODUCTION.....	5
II. GENERATION AND TIME DECAY OF GAS PHASE O_2F	13
III. REACTION SURVEY.....	23
1. Reactions Producing Excited BrF	23
2. Reactions Producing Excited IF	35
3. O_2F Reactions with $Mg(^1S)$ and $Mg^*(^3P)$	44
4. The Reaction of Calcium with O_2F	65
IV. CONCLUSIONS.....	73
V. REFERENCES.....	76

LIST OF ILLUSTRATIONS

1. O_2F ultraviolet absorption spectrum.....	14
2. Apparatus used for measurement of the time decay of O_2F	18
3. Second order plot for O_2F decay.....	20
4. Modified apparatus used for observation of reactions of O_2F with added gases.....	24
5. $BrF\ B(^3\Pi_0^+) \rightarrow X(^1\Sigma^+)$ emission spectrum.....	27
6. $BrF\ B \rightarrow X$ photon yield vs the flowrate of bromine atoms.....	34
7. IF emission spectrum showing $A(^3\Pi_1) \rightarrow X(^1\Sigma^+)$ and $B(^3\Pi_0^+) \rightarrow X(^1\Sigma^+)$ transitions.....	39
8. Apparatus used for generation of magnesium vapor.....	47
9. Apparatus used for observing the reaction of O_2F with magnesium.....	48
10. Calibration of the flowrate of magnesium vs temperature.....	50
11. Broadband emission observed from the $Mg + O_2F$ reaction.....	53
12. Spectrum of $MgF\ A(^2\Pi) \rightarrow X(^2\Sigma^+)$ emission.....	55
13. Photon yield of the broadband emission vs the flowrate of magnesium.....	58

LIST OF ILLUSTRATIONS (Continued)

	Page
14. Photon yield of the MgF A + X emission vs the flowrate of magnesium.....	59
15. Cells used for observation of the reaction of Mg [*] (³ P) with O ₂ F.....	62
16. Spectra of emissions from the reaction of O ₂ F with Mg(¹ S)/Mg [*] (³ P).....	64
17. Calibration of the flowrate of calcium vs temperature.....	67
18. Spectrum of Ca + O ₂ F chemiluminescence in the visible region.....	69
19. Spectrum of Ca + O ₂ F chemiluminescence in the ultraviolet region.....	71

LIST OF TABLES

I. Results of O ₂ F Time Decay Measurements.....	21
II. ⁷⁹ BrF - ⁸¹ BrF Isotope Splittings Observed for the B(³ Π ₀ ⁺) + X(¹ Σ ⁺) Transition.....	29
III. Deslandres Table for the A(³ Π ₁) + X(¹ Σ ⁺) Transition of IF.....	40

I. INTRODUCTION

The development of lasers based upon direct chemical pumping of population inversions among electronically excited states requires that two broad groups of conditions be met. The first such group pertains to the reaction; i.e., formation of the inversion. Either the dynamic constraints on the reaction must be such that excited product states are preferentially populated, or the spectroscopy of the system must be such that populated upper levels are optically connected to unpopulated lower levels (e.g., by favorable Franck-Condon shifts). In addition, the speed of the reaction must allow the production of excited products to compete well with deactivation mechanisms. The second condition pertains to the nature of the excited species: it must be suitable for lasing. The radiative lifetime of the excited state formed must be short enough to allow reasonable gain but not so short as to preclude build-up of the inversion density. The density of states in the levels populated by the reaction should be as low as possible (such that "dilution" of the inversion density is minimized), and intramolecular and intermolecular deactivation processes must not be efficient.

It is clear that progress in this area requires a judicious choice of candidate lasing species, and a number of atoms and molecules have risen to the forefront of attention in this regard. Many of these are diatomic fluorides, e.g., interhalogens, group VA fluorides, and metal fluorides. The potential of the interhalogen systems stems in part from the metastability of the lowest lying excited electronic states, $A^3\Pi_1$ and $B^3\Pi_0^+$, which are

connected to the ground $1\Sigma^+$ state by forbidden singlet-triplet transitions. The radiative lifetimes of the B states of these species have been found to be on the order of 10^{-5} seconds (Ref. 1), with the lifetime of the A states being one to two orders of magnitude greater (Ref. 2, 3). Also, these excited triplet states exhibit strong Franck-Condon shifts. For IF, $v' = 0$ of the B state is connected to $v'' = 4$ and 5 of the ground state (Ref. 2). This displacement is even more pronounced for BrCl, for which transitions to $v'' = 16-18$ are favored (Ref. 4). These attributes have led to an extended investigation of the chemical production of $\text{BrCl}^*(3\Pi_0^+)$ at the AFWL (Ref. 5) and to the demonstration of a number of optically pumped molecular halogen lasers (Ref. 6, 7).

The chemical production of excited Group VA fluorides has been investigated (with quite promising results) in this laboratory (Ref. 8) as well as others (Ref. 9). The potential of these systems is based upon the preferential production of metastable triplet states by strongly spin-constrained reactions (Ref. 10), with the subsequent emission occurring in very narrow bandwidths. Numerous reactions producing excited metal fluorides have been investigated (Ref. 11, 12). These systems are of interest because of the highly energetic nature of $\text{M} + \text{F}_2$ (or RF) reactions, typically accessing many excited product states. Owing to the ionic nature of metal fluorides, production of excited species in these reactions generally occurs by curve-crossing mechanisms.

The work described herein was directed toward assessing the utility of gas phase O_2F radicals as a reagent for the production of electronically excited diatomic fluorides. The O_2F molecule is one in which the fluorine atom is very weakly bound to the O_2 moiety. The strength of the O-F bond in this

species has been estimated to be on the order of 15 kcal/mole (Ref. 13, 14). The O-O bond strength is ~110 kcal/mole (Ref. 14) (i.e., only slightly weaker than in a free O_2 molecule). Owing to the lability of the fluorine atom, the reactions of O_2F may liberate a very large amount of energy (~22 kcal/mole more than analogous processes involving F_2). Such reactions may in fact be similar to three-body recombinations (with the O_2 acting as the third body) in their ability to form excited states, but should proceed with the speed of rapid bimolecular processes.

The O_2F radical is unusually stable and has been well characterized in liquid solutions (Ref. 15) and solid matrices (Ref. 16) at cryogenic temperatures. It has been observed in the gas phase from flash photolysis of O_2 - RF mixtures at high pressures (hundreds of torr) (Ref. 17, 18). In such an environment, fluorine atoms produced by the flash combine with oxygen at a rate about two orders of magnitude greater than $F+F+M$ recombination. Based on this kinetic situation, the formation of O_2F has been used to monitor the quantum yields for F atom production by the photolysis of RI compounds (Ref. 18). The EPR and IR spectra of the radical are known from the condensed phase experiments mentioned above. The UV spectrum in the gas phase, dominated by a strong absorption in the vicinity of 210 nm, was measured in the F_2 - O_2 flash photolysis experiments.

In the experiments performed in our laboratory, gaseous O_2F was produced by the thermal decomposition of solid $O_2^+AsF_6^-$:

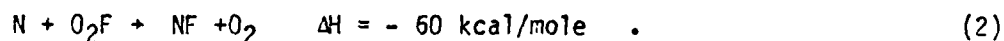


This material was synthesized for these experiments at the Rocketdyne Division of Rockwell International by the photolysis of mixtures of O_2 , AsF_5 , and F_2 contained in a quartz vessel. In this procedure the dioxygenyl salt forms as a precipitate on the vessel walls. Some of the material used early in the program was prepared by applying heat to gas mixtures contained in stainless steel vessels; this procedure was abandoned in favor of the photolysis since the solid precipitate clogged the valve of the metal vessel. Subsequent handling of the $\text{O}_2^+\text{AsF}_6^-$ salt was done either under vacuum or in a dry box, since it reacts vigorously with water vapor present in the air.

The final decomposition products of $\text{O}_2^+\text{AsF}_6^-$ have been shown to be O_2 , F_2 , and AsF_5 (Ref. 19). In their study of the decomposition of the similar salt $\text{O}_2^+\text{BF}_4^-$, however, Kieth and co-workers inferred an initial equilibrium involving gaseous O_2F and BF_3 (Ref. 20). One would expect similar behavior from the arsenic salt and indeed the data presented below confirm this hypothesis. In our experiments, the presence of O_2F downstream of the decomposing solid was monitored using its strong UV absorption near 210 nm. Chegodaev, et. al., have reported an $\epsilon_{\text{max}}(\text{O}_2\text{F})$ of $\sim 10^4 \text{ l mole}^{-1}\text{cm}^{-1}$ at $\sim 206 \text{ nm}$ (Ref. 17). Among the gas phase species possibly produced by decomposition of the salt (AsF_5 , O_2F , O_2 , F_2 , and less probably F and O_2F_2), only O_2F and O_2F_2 have appreciable absorptions at the wavelength. Since $\epsilon(\text{O}_2\text{F}) \gg \epsilon(\text{O}_2\text{F}_2)$ in this region (Ref. 17), only absorptions due to O_2F were observed in our experiments. The strength of the absorptions observed (for a given pressure increase

caused by decomposition of the salt) were roughly commensurate with the reported magnitude of the O_2F extinction coefficient.

Techniques for the generation of O_2F from $O_2^+AsF_6^-$ and for the observation of its reactions with added species were developed in experiments performed prior to the beginning of this contract. The first such experiments involved the reaction of active nitrogen with O_2F (Ref. 21). One would expect the production of NF in this system via a highly exothermic process:

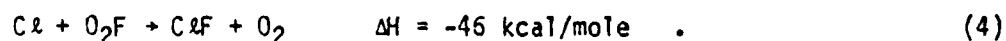


The most striking result of these experiments, however, was a dramatic enhancement (by a factor of 50 or more) of the N_2^* first positive ($B^3\Pi_g \rightarrow A^3\Sigma_u^+$) emission when O_2F was present. The intensity distribution of the enhanced N_2^* emission was strongly shifted to the red relative to the normal Lewis-Rayleigh afterglow. Only very weak NF^* ($b^1\Sigma^+ \rightarrow X^3\Sigma^-$) emission was observed. Deconvolution of the data to yield the steady state vibrational populations of the N_2^* $B(^3\Pi_g)$ state showed the results to be consistent with a mechanism in which reaction (2) above forms excited NF in the $^1\Delta$ or $b^1\Sigma^+$ states, which subsequently react with another nitrogen atom to form excited N_2 :



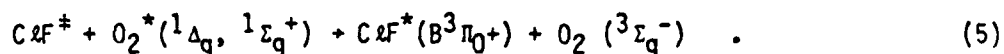
The weakness of the NF^* emission in this system argues that $k_3 \gg k_2$.

More detailed observations were made of the reaction of chlorine atoms with O_2F (Ref. 22). The initial reaction between these two species is insufficiently exothermic for direct production of the lowest lying excited electronic states ($A^3\Pi_1$ or $B^3\Pi_0^+$) of ClF :



Although the energy of the ClF A state is unknown, comparison to other interhalogens suggests that it would not be accessible by reaction (4). Indeed, no emission was evident in the experimental observation of the system, unless excited singlet molecular oxygen ($O_2^* \ ^1\Delta_g, \ ^1\Sigma_g^+$) produced from a microwave discharge was also admitted to the flow. In this case, a bright orange flame was generated, the emission spectrum of which indicated the predominance of ClF $B \rightarrow X$ transitions. These experiments represent the first observation of $B \rightarrow X$ emission from the ClF molecule. Due to the weakness of this transition, the only previous such data had been obtained from absorption studies using high pressures (hundreds of torr) and pathlengths up to 4 m (Ref. 23, 24). Analysis of the emission spectrum obtained in our experiments resulted in calculation of the most precise values of the molecular constants of the B and X states of ClF currently available.

From the behavior of the system with respect to the added singlet oxygen, it was inferred that the excited ClF was produced by a two step mechanism as follows:



Energy transfer processes analogous to reaction (5) have been previously suggested for other halogen and interhalogen systems (Ref. 2, 28). The identity of the intermediate ClF^\ddagger is unknown at present; it may be either a highly vibrationally excited ground state molecule or an electronically excited species in one of the metastable states of the $^3\Pi$ manifold. The issue of the identity of this intermediate is addressed further by the data presented below.

The utility of O_2F in a potential laser system is a function of both the efficient production of excited species and the ability to generate sizable concentrations of the O_2F reagent. Hence, the program described below was divided into two basic tasks as follows:

1. O_2F Generation and Diagnostics. The goal of this task was the development of a calibrated and standardized source of O_2F to be used in reaction studies, and the determination of the lifetime of O_2F in the gas phase.
2. Reaction Survey. This task involved the analysis of chemiluminescence spectra and measurement of photon yields for the reactions of O_2F with atomic and molecular halogen and metal atoms.

After a number of iterations, a standardized O_2F cell was developed and the temporal behavior of the radical in the cell was determined. This apparatus was subsequently used for the observation of O_2F reactions producing electronically excited BrF and IF . A separate apparatus was constructed for metal + O_2F systems and it was subsequently used to observe reactions producing excited MgF and CaF . Chemiluminescence spectra and photon yields were measured for these reactions, and a number of new and unexpected results were obtained.

II. O_2F GENERATION AND DIAGNOSTICS

In the experiments noted above, the presence of gaseous O_2F downstream of the decomposing $O_2^+AsF_6^-$ was inferred from the strong absorption by the radical of light in the vicinity of 210 nm. In the first part of our effort on this task, we obtained additional support for this inference by measurement of the UV absorption spectrum of the gas phase decomposition products of the salt. The cell used for these measurements was that previously used in the C $_2$ F experiments (described in detail in Reference 22), since it provides an absorption pathlength of ~20 cm. O_2F was generated at either end of the cell with the vacuum connection in the center. For the pressures used in the experiments, the residence time in the cell was less than 2 msec. The light source used was an Oriel deuterium lamp. An iris was placed in front of the lamp such that only a thin pencil of the relatively high intensity beam was admitted to the cell. The lamp transmission was measured using a 0.12 m Oriel monochromator with 500 μ m slits and an RCA IP28 photomultiplier tube whose response was monitored by a Kiethley 610B electrometer. The spectrum was obtained from comparison of the transmission with no heat applied to the $O_2^+AsF_6^-$ reservoirs vs the transmission through a steady flow of decomposition products.

Five independent measurements of the spectrum were made, and all showed a broadband absorption peaking near 210 nm. No evidence of structure was observed within the resolution of the monochromator (~3.2 nm). Figure 1 shows a typical result as a plot of $\log(I_0/I)$ vs wavelength. Also shown is

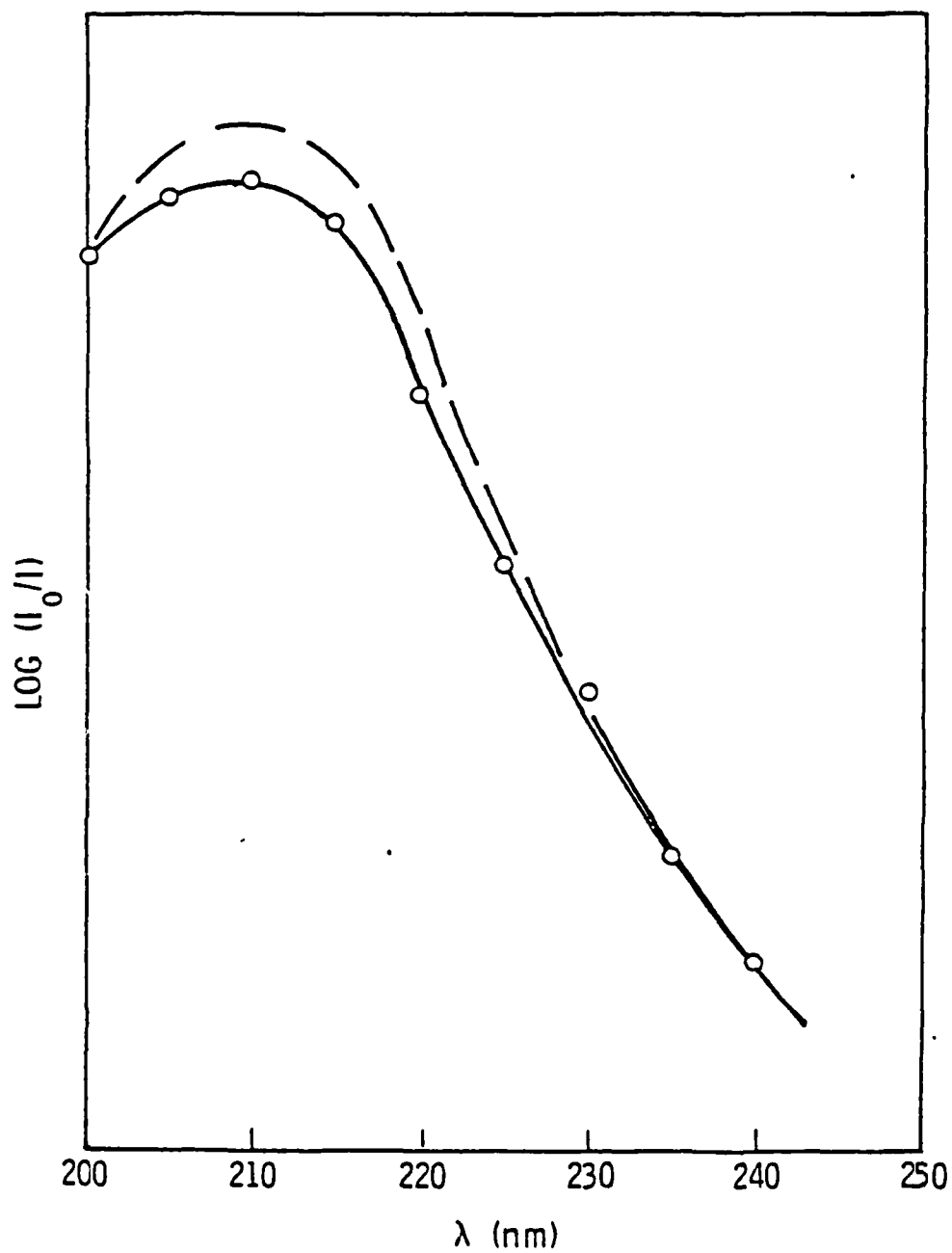


Figure 1. UV absorption spectrum of the gas phase products of the thermal decomposition of $\text{O}_2^+\text{AsF}_6^-$ (solid line). The O_2F_2 absorption spectrum reported in reference 17 is shown as a broken line.

the O_2F absorption spectrum obtained by Chegodaev, et. al., from the flash photolysis of $RF + O_2$ mixtures (Ref. 17, 18). The two spectra, which have been normalized in the figure at 200 nm, clearly agree with one another. This is strong evidence that O_2F is in fact the species responsible for the absorption.

Accurate values of extinction coefficients could not be determined from our experiments due to the inexact pathlength and uncertainty in the O_2F concentration (some fraction of the radicals were undoubtedly removed on the walls of the 10 mm diameter vessel during transit). Assuming, however, an upper limit on the O_2F concentration equal to half the pressure rise caused by $O_2^+AsF_6^-$ decomposition, the extinction coefficient at the maximum absorption (206 nm) is greater than $5 \times 10^3 \text{ } \mu\text{mole}^{-1}\text{cm}^{-1}$. The extinction coefficient reported from the $RF + O_2$ photolysis experiments was $\epsilon_{\text{max}} = 1 \times 10^4 \text{ } \mu\text{mole}^{-1}\text{cm}^{-1}$ (Ref. 17).

The authors of the flash photolysis studies reported that in their experiments the decay of O_2F could be described by a second order rate equation (Ref. 17, 26). A decay mechanism involving five elementary processes was proposed. Termolecular reactions were included since the experiments were carried out at pressures greater than 250 torr. The mechanism suggests that the second order behavior is brought about by a combination of first order effects rather than by an $O_2F + O_2F$ elementary reaction, and the authors rule out the participation of a direct second order process. Consideration of the conditions of our experiments (pressures less than 1 torr and small O_2 concentrations) reduces the mechanism to a two step decay as follows:





Hence, for a steady-state fluorine atom concentration, the mechanism would predict a simple first order decay dependent on the total pressure.

An alternative point of view is presented by Kieth, et. al. (Ref. 20), in their investigation of the thermal decomposition of dioxygenyl fluoroborate ($\text{O}_2^+\text{BF}_4^-$), a species similar to the $\text{O}_2^+\text{AsF}_6^-$ salt used in the present experiments. These authors' results suggest that this salt decomposes via an equilibrium with O_2F and BF_3 , in accord with the present experiments:



An analysis of the kinetics of the formation of BF_3 in the system was shown to be consistent with removal of O_2F from the equilibrium by a second order ($\text{O}_2\text{F} + \text{O}_2\text{F}$) elementary process.

Measurement of the time decay of O_2F produced in our experiments requires that the concentration of the radical be measured simultaneously at individual points along the length of a flow tube. This requirement severely constrains the experimental apparatus, since the O_2F concentration and/or the absorption pathlength must be large enough to yield significant absorptions while the flow tube cross-sectional area must be small enough to maintain appropriate linear flow velocities. The apparatus developed for these experi-

ments is shown in Figure 2. The rectangular cell has internal dimensions 5.1 x 1.3 cm. The $\text{O}_2^+\text{AsF}_6^-$ salt rests on two coarse fritted discs of ~1 cm diameter which are positioned in 1 cm tubes about 2.5 cm below (upstream of) the rectangular section of the cell. In the experiments, N_2 was passed through the frits to carry the decomposition products of the $\text{O}_2^+\text{AsF}_6^-$ into the flow stream. N_2 was also added to the flow above the frits to increase the total pressure and linear velocity in the cell (see below). The entire cell, frit area, and N_2 flow lines were heated using conventional heating tapes to cause decomposition of the salt and hence generation of O_2F . The walls of the rectangular cell were heated to prevent fogging.

O_2F concentrations were monitored by measuring the absorption across the long dimension of the cell. For these experiments, the collimated output of an electrodeless I_2 lamp (206.2 nm line) was split into three beams which were passed through the cell at positions spaced 3.8 cm apart. The intensities of the three beams were individually monitored by an array of IP28 photomultiplier tubes. The open aperture to each PMT was covered by a narrow band interference filter (Acton Research Corp.) centered at 210 nm. The responses of the detectors were simultaneously monitored by three electrometers and recorded on strip chart recorders.

The linear velocity of the flowing gases in the cell was calibrated vs pressure by passing N_2 through the system via a Tylan FM-400 mass flowmeter. Pressures were monitored at either end of the rectangular cell using an MKS Baratron capacitance manometer (see Fig. 2). The measurements showed that

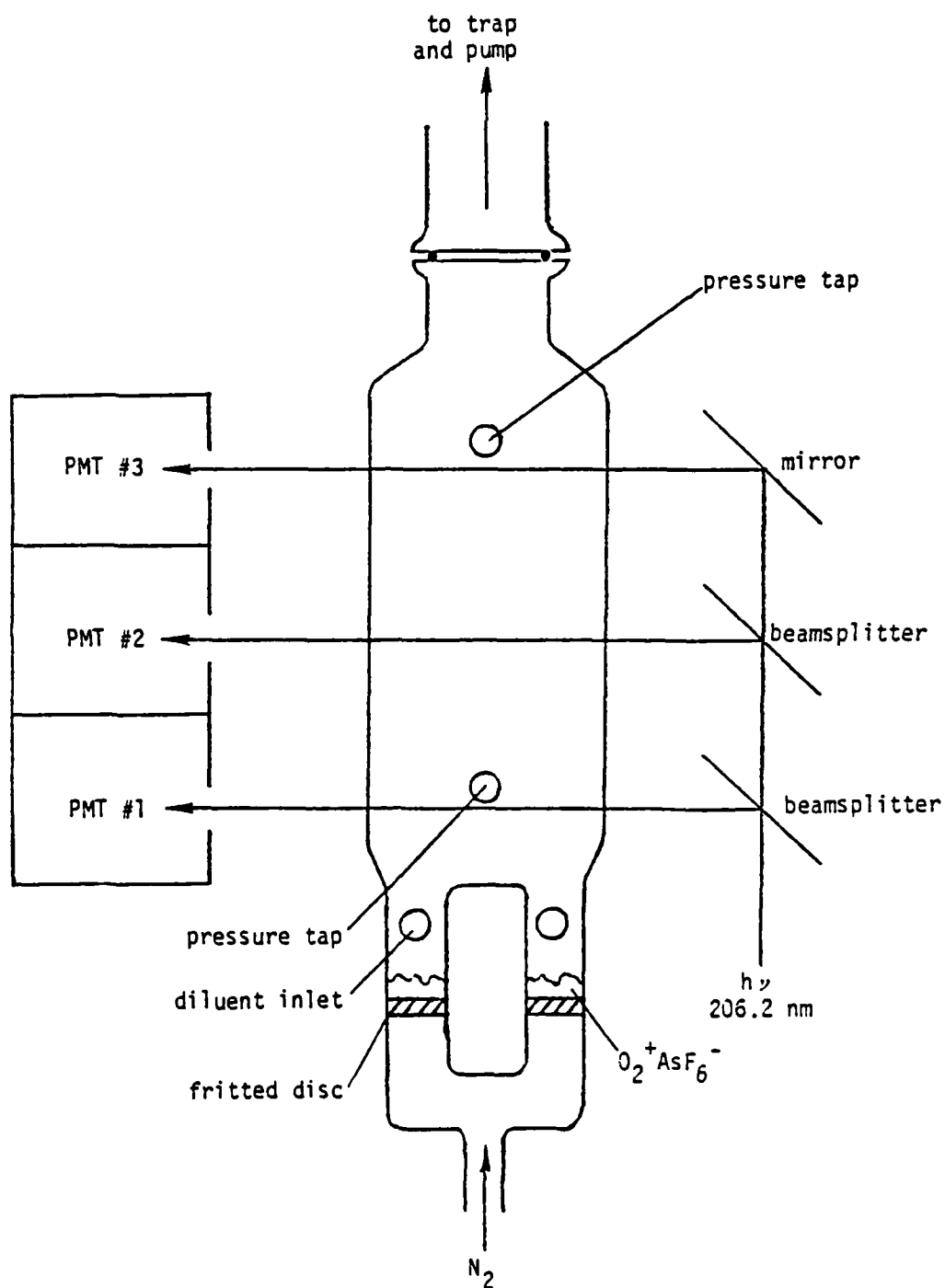


Figure 2. Apparatus used for measurement of the time decay of gas phase O_2F .

the pressure drop down the rectangular section was negligible. There was, however, a considerable variation of the linear velocity with pressure and hence the time between the points of the absorption measurement could be controlled by the amount of diluent added to the flow. For typical pressures used in the experiments, the time between each of the measurement points was 6 to 10 msec.

The O_2F concentration at each point was calculated from the measured absorption and the extinction coefficient reported in Reference 17, $\epsilon_{206} = 1 \times 10^4 \text{ l mole}^{-1} \text{ cm}^{-1}$. The exact time separation of the measurements was determined from the total pressure. Since absorptions at all three points were continuously monitored in time, calculations were made for several times during a given experiment. Five such experiments were performed. There was some scatter in the data, resulting in a degree of uncertainty with regard to the order of the decay of O_2F . Many measurements were made, however, and in general the best agreement was obtained assuming a second order decay mechanism. Also, variations in the total pressure in the cell (by as much as 30%) were not reflected in the decay rates. Figure 3 shows a second order plot ($[O_2F]^{-1}$ vs t) for a typical experiment. In each case it was noted that measurements made during the rise of the absorption resulted in anomalously large slopes; more consistent results were obtained for the larger absorptions occurring later in the run.

Table I shows a compilation of all the values of k (23 results) for runs which gave measurable absorptions. In determining an average, 3 of the 23 values were rejected since their deviation from the mean of the remaining 20

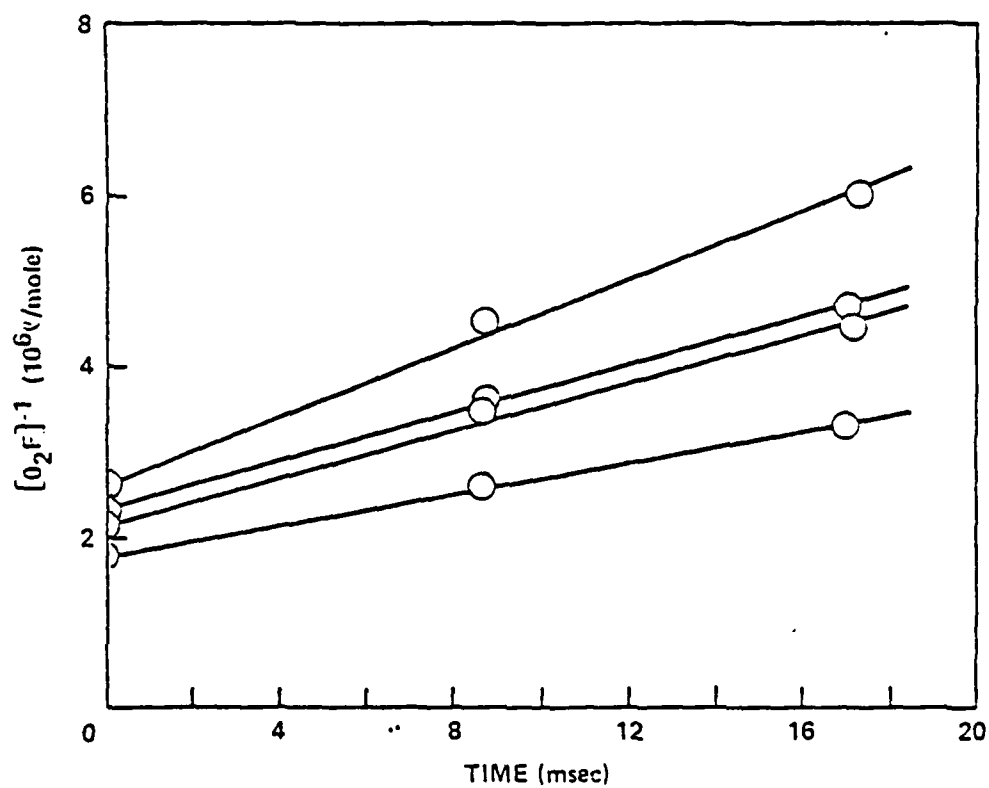


Figure 3. Second order plot of the time decay of O_2F for a particular run. Each of the lines represents data taken at a different time during the run.

TABLE I

RATE CONSTANT FOR O₂F SECOND ORDER REMOVAL

Run No.	T _x (b)	k (cm ³ mole ⁻¹ sec ⁻¹)
1B	T ₁	2.72 x 10 ¹¹ (a)
	T ₂	2.00 x 10 ¹¹
	T ₃	1.43 x 10 ¹¹
	T ₄	1.38 x 10 ¹¹
	T ₅	0.94 x 10 ¹¹
2B	T ₂	1.25 x 10 ¹¹
	T ₃	0.94 x 10 ¹¹
	T ₄	0.99 x 10 ¹¹
	T ₅	0.88 x 10 ¹¹
5B	T ₂	2.50 x 10 ¹¹ (a)
	T ₃	1.77 x 10 ¹¹
	T ₄	1.40 x 10 ¹¹
	T ₅	1.70 x 10 ¹¹
5D	T ₁	1.63 x 10 ¹¹
	T ₂	1.34 x 10 ¹¹
	T ₃	1.00 x 10 ¹¹
	T ₄	1.44 x 10 ¹¹
	T ₅	2.00 x 10 ¹¹
	T ₆	2.75 x 10 ¹¹ (a)
5E	T ₁	1.31 x 10 ¹¹
	T ₂	1.19 x 10 ¹¹
	T ₃	1.13 x 10 ¹¹
	T ₄	1.25 x 10 ¹¹

$\langle k \rangle = 1.4 \pm 0.4 \times 10^{11} \text{ cm}^3 \text{ mole}^{-1} \text{ sec}^{-1}$

a. Values not included in final average (see text).

b. T_x indicate measurements made at different times during a given run.

points was greater than 4 times the average deviation of those points. The resultant value of k is $1.4 \pm 0.4 \times 10^{11} \text{ cm}^3 \text{ mole}^{-1} \text{ sec}^{-1}$.

The observed second order decay could result from an $\text{O}_2\text{F} + \text{O}_2\text{F}$ reaction, or from the removal of O_2F by AsF_5 via an equilibrium analogous to process (8) above:



This latter possibility seems unlikely, however, since the entire cell was heated well beyond the observation zone and there was no evidence of re-deposited $\text{O}_2^+\text{AsF}_6^-$ solid downstream of the reservoirs. Hence, the present results suggest that either some discrepancy exists between the flash photolysis and thermal decomposition results, or that the decay mechanisms in these experiments are fundamentally different from one another.

Since the half-time of a second order process is given by $t_{1/2} = (kC_0)^{-1}$, an initial concentration of ~ 150 mtorr of O_2F would decay to half its value in ~ 1 msec. Hence, O_2F would appear to be a suitable reagent for use in moderate to high gain laser systems. It is likely not to be useful, however, for low gain systems requiring concentrations of excited species greater than 10^{16} molecules/cm³.

III. REACTION SURVEY

1. Reactions Producing Excited BrF

As noted in the discussion above, halogen monofluorides are among the most promising of all diatomic fluorides with respect to their potential for sustaining lasing in the visible and near IR regions of the spectrum. Hence, the reactions of O_2F with halogen atoms were among the first that we chose to study.

In contrast to the ClF case discussed above, a wealth of spectroscopic data exists concerning the $B \rightarrow X$ transitions in BrF and IF . Detailed studies of these transitions involving chemiluminescence (Ref. 25, 27), absorption (Ref. 28, 29), and laser induced fluorescence (Ref. 30, 31) techniques have been published by a number of authors. In addition, observations of the $A(^3\Pi_1) \rightarrow X(^1\Sigma^+)$ transition have been reported for both BrF (Ref. 29) and IF , (Ref. 2) although the BrF measurement has been the subject of some controversy (Ref. 32) and has not been reproduced. In view of the existence of this large body of spectroscopic information, the primary thrust of the present experiments was directed toward the nature and efficiency of the mechanisms producing the excited species. The results obtained, however, clearly demonstrated the potential of the O_2F reactions for producing detailed spectroscopic information.

Observations of O_2F reactions using the cell developed for absorption measurements (Fig. 2) required modifications to be made for rapid mixing of the reagents. The modified cell is shown in Figure 4. Reagents were added to

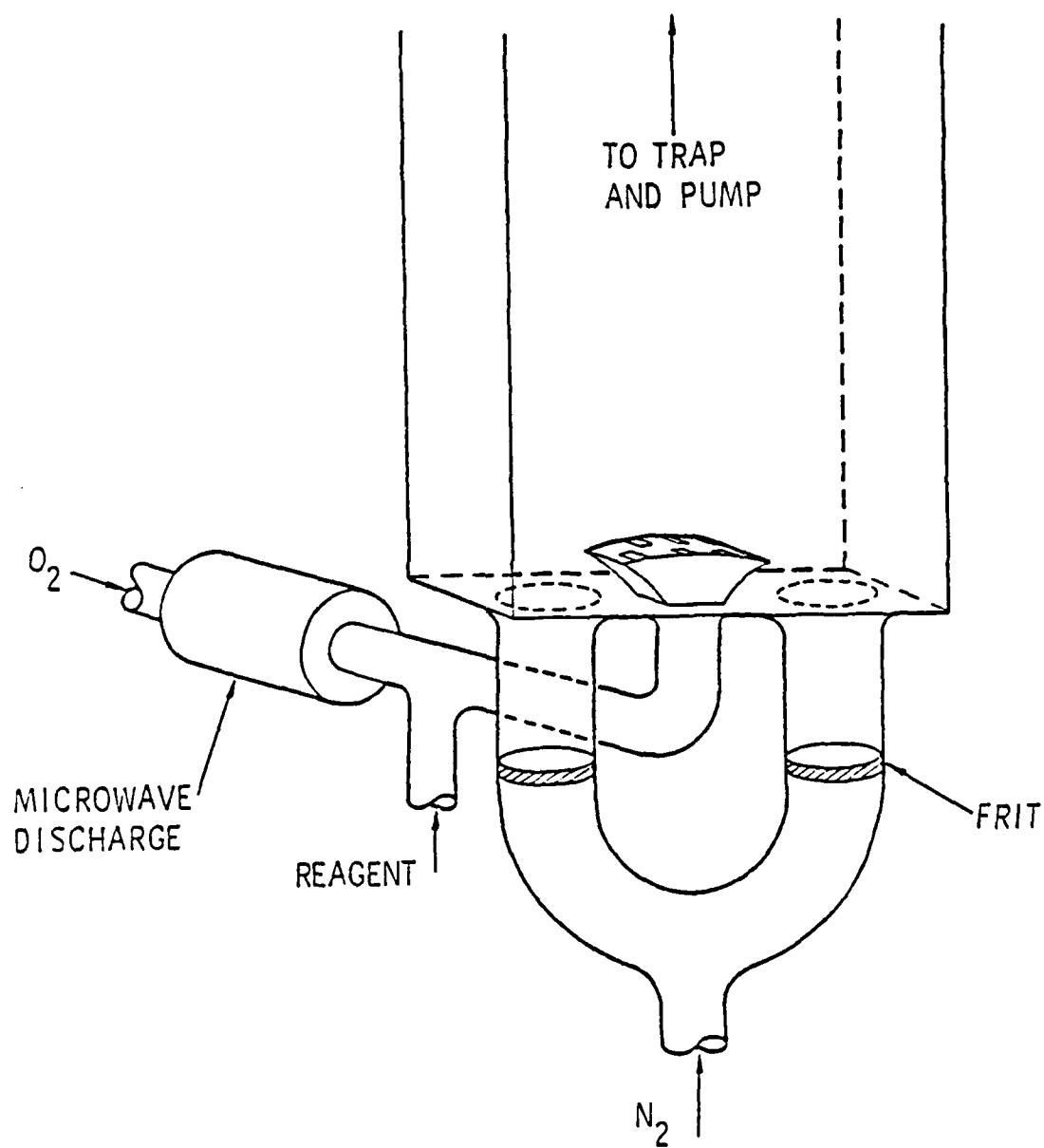
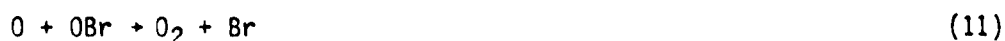


Figure 4. Modified apparatus (see Figure 2) used for observation of the reactions of O_2F with added gases.

the cell through a wedge shaped injector positioned between the two O_2F entry ports. The injector incorporated an array of slots through which reagents passed into the stream. Visual inspection of flames produced in the cell indicated that this arrangement resulted in rapid mixing. Emissions from within the cell were dispersed by a McKee-Pederson 0.5 m monochromator and detected by a photon counting apparatus consisting of a cooled RCA C31034 photomultiplier tube, a PAR-1120 amplifier-discriminator, and an SSR-1110 counting unit. The entrance slit of the monochromator was positioned such that the cone of sight passed through the short (1.3 cm) dimension of the cell directly over the reagent injector. The time duration of flames produced in the cell was monitored by an array of three RCA IP28 photomultiplier tubes positioned along the length of the cell.

BrF experiments were performed by adding a mixture of Br_2 in Argon (~ 10 mtorr) to a stream of diluent oxygen (~ 250 mtorr) just upstream of the cell, as shown in Figure 4. Liquid Br_2 was purified by multiple freeze-pump-thaw cycles at 196 K and the mixture with argon (Matheson U.H.P., 99.999%) was prepared in a 35 l vessel prior to use in the experiments. The mixture contained $\sim 19\%$ Br_2 . Addition of these gases to O_2F generated in the cell (< 15 mtorr) produced a very faint luminescence which was barely visible to the eye. The spectrum of this emission (recorded at the detection limits of our apparatus) showed it to be due to $B(^3\Pi_0^+) \rightarrow X(^1\Sigma^+)$ transitions in BrF. Experiments were also performed in which the O_2 was passed through an 80 W microwave discharge prior to mixing with the Br_2 . In this case, bromine atoms are produced quantitatively by the rapid reactions (Ref. 33)



These experiments produced an extremely intense yellow emission which was clearly visible in the lighted room. A low resolution scan of the yellow emission, shown in Figure 5, indicated that it was also due to BrF B \rightarrow X transitions.

The yellow flame was well-defined and decayed within 3 cm of the injector, corresponding to a decay time $\tau < 5$ msec. For a typical flow velocity of ~ 600 cm sec⁻¹, the time frame of B(³ π_0^+) spontaneous emission (< 40 usec)¹ is such that the average excited molecule travels less than 0.3 mm before radiating. Hence the observed decay time (~ 3 cm) must be due to the processes which limit formation of the excited species (e.g., mixing and the finite reaction rate). Given that the O₂F concentration in these experiments was less than 5×10^{14} molecules cm⁻³, the decay time sets a lower limit on the formation rate of $k > 2 \times 10^{11}$ cm³ mole⁻¹ sec⁻¹. Hence the data indicate that excited BrF is produced by rapid bimolecular processes rather than by three-body recombination. Recombination processes occurring in our cell at comparable pressure were observed to yield flames lasting for many msec (extending well beyond the cell and into the trap). The BrF flame exhibited a sharp intensity peak with respect to the Br₂/Ar flowrate. The peak intensity was many times (two or three orders of magnitude) greater than that produced by the similar C₂-O₂F-O₂^{*} reaction. The BrF flame was completely quenched at Br₂

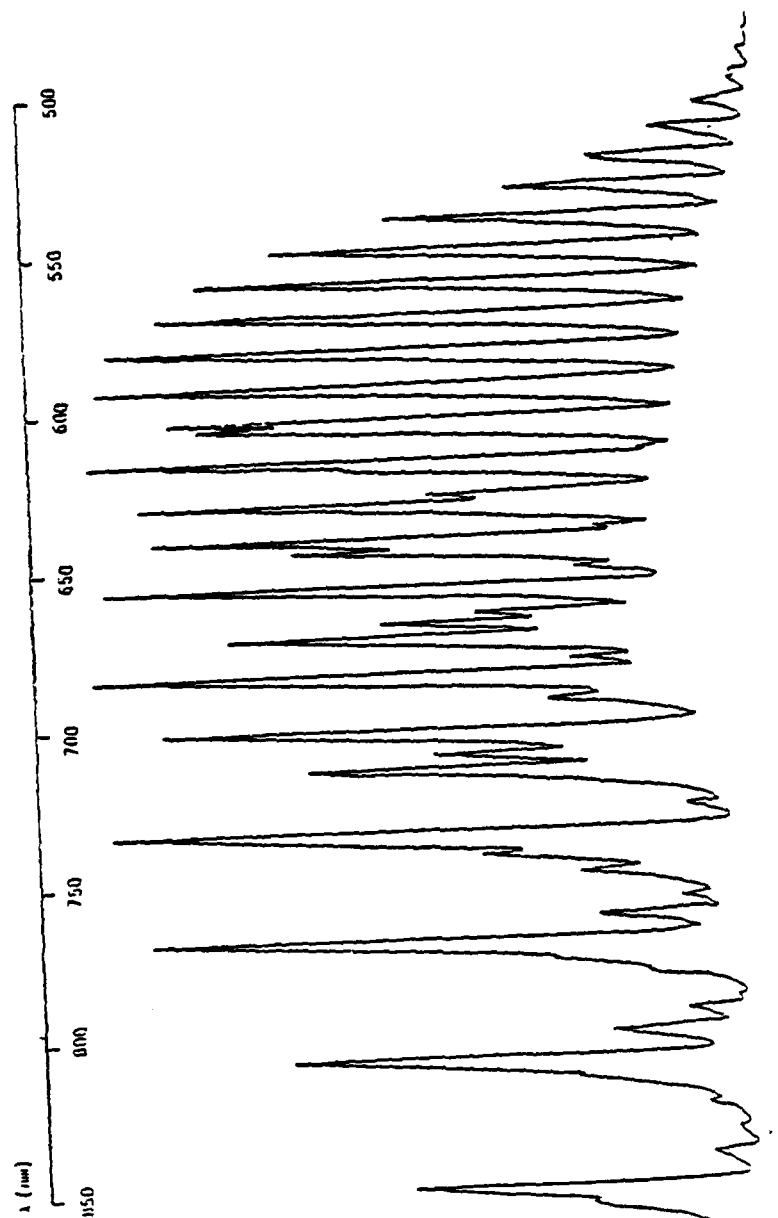


Figure 5. $\text{BrF } B(3\Pi_0^+) \rightarrow X(1\Sigma^+)$ emission spectrum.

flowrates only slightly greater than that which yielded the brightest flame. This behavior is consistent with the observations by Clyne and McDermid that BrF $B(^3\Pi_0^+)$ is quenched efficiently by collisions with either Br₂ or ground state BrF (Ref. 34).

The BrF emission spectrum was recorded using the photon counting apparatus described above. Scans of the spectrum were made at 5 nm per minute with a counting interval usually less than 0.1 sec and a slitwidth of 100 μ m. Eight scans were made, covering the region 450 nm to 900 nm. The spectrum consisted of 63 red-degraded bands, all of which could be assigned to $B(^3\Pi_0^+) \rightarrow X(^1\Sigma^+)$ transitions in BrF. Well resolved rotational structure was observed in many of the bands, and the ^{79}BrF - ^{81}BrF isotope splitting was resolved for 22 bands of the long wavelength side of the spectrum. No previously unreported bands were observed, however, and no bands corresponding to possible $A(^3\Pi_1) \rightarrow X(^1\Sigma^+)$ transitions were present in the spectrum. In general, the data agree well with the spectrum reported by Clyne and co-workers for BrF produced by recombination in the presence of excited singlet oxygen (Ref. 25). There were, however, some notable differences in the frequencies of bands occurring at longer wavelengths. Clyne et al., did not resolve the isotope splitting for these bands, and suggested that the measured frequencies probably corresponded most closely to transitions in ^{79}BrF . Our data show that a number of the frequencies reported by these authors actually correspond to ^{81}BrF bands. Since the isotope splittings for the longer wavelength bands have not been previously reported, we have compiled these frequencies in Table II. Also shown are calculated values for the splittings ($\Delta\nu$) using the theoretical value of

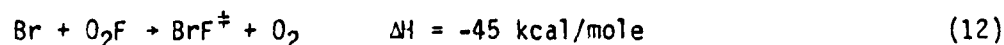
TABLE II
OBSERVED ISOTOPE SPLITTINGS IN THE
BrF B($^3\Pi_0^+$) \rightarrow X($^1\Sigma^+$) EMISSION SPECTRUM^a

Band	^{79}BrF	^{81}BrF	$\Delta\nu$	$\Delta\nu_{\text{calc}}^b$
0,4	15517 \pm 2	15522 \pm 2	5 \pm 2	6.6
1,5	15252 \pm 2	15259 \pm 2	7 \pm 2	7.3
4,7	15052 \pm 2	15063 \pm 2	9 \pm 2	7.7
0,5	14883 \pm 2	14893 \pm 2	10 \pm 2	8.1
1,6	14629 \pm 2	14636 \pm 2	7 \pm 2	8.7
0,6	14259 \pm 2	14269 \pm 2	10 \pm 2	9.6
1,7	14013 \pm 2	14021 \pm 2	9 \pm 2	10.2
0,7	13642 \pm 2	13654 \pm 2	12 \pm 2	10.2
3,9	13510 \pm 4	13521 \pm 4	11 \pm 4	11.4
1,8	13408 \pm 4	13417 \pm 4	9 \pm 4	11.7
2,9	13157 \pm 2	13170 \pm 2	13 \pm 2	12.2
0,8	13032 \pm 2	13044 \pm 2	12 \pm 2	12.5
4,11	12666 \pm 2	12680 \pm 2	14 \pm 2	13.4
2,10	12568 \pm 2	12581 \pm 2	13 \pm 2	13.7
0,9	12435 \pm 2	12448 \pm 2	13 \pm 2	14.0
1,10	12212 \pm 3	12227 \pm 3	15 \pm 3	14.5
4,12	12094 \pm 3	12106 \pm 3	12 \pm 3	14.8
2,11	11986 \pm 2	12000 \pm 2	14 \pm 2	15.1
0,10	11844 \pm 2	11858 \pm 2	14 \pm 2	15.4
3,12	11760 \pm 3	11774 \pm 3	14 \pm 2	15.6
1,11	11629 \pm 3	11644 \pm 3	15 \pm 2	16.0
0,11	11260 \pm 2	11275 \pm 2	15 \pm 2	16.8

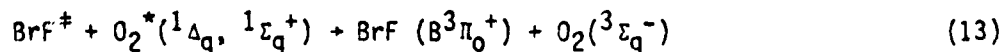
a. Frequencies reported in vacuum wavenumbers.
b. Splittings calculated using $\rho = 0.9976$.

$\rho = [\mu(^{79}\text{BrF})/\mu(^{81}\text{BrF})] = 0.9976$. The agreement is generally good (note that systematic contributions to the uncertainties of the transition frequencies do not apply to the splittings). Calculation of ρ from the sum of the data as in Reference 22 yields $\rho = 0.9977$, in good agreement with the theoretical value.

It seems likely that the mechanism responsible for production of excited BrF in the $\text{Br-O}_2\text{F-O}_2^*$ system is the same as that which has been proposed for C&F ($\text{B}^3\Pi_0^+$) formation in the $\text{Cl-O}_2\text{F-O}_2^*$ system (Ref. 22). As in the C&F case, the initial reaction between bromine atoms and O_2F is insufficiently exothermic for direct production of either the $\text{A}^3\Pi_1$ or $\text{B}^3\Pi_0^+$ states of BrF:



Here we have assumed the O-F bond strength in O_2F to be about 15 kcal/mole (Ref. 13, 14). We postulate that reaction (12) forms an excited intermediate BrF^\ddagger which is subsequently pumped to the B state by collisions with singlet oxygen:



The efficiency with which the B state is formed may be a strong function of the nature of BrF^\ddagger . If it is a vibrationally excited species, the fraction pumped to the B state will be determined to some extent by the initial distribution among vibrational levels and the speed at which these excited levels

relax. It seems likely that in this case the fractional production of the B state will be low. If, on the other hand, the intermediate is an excited electronic state formed preferentially because of some dynamic constraint on the reaction, the efficiency for production of the B state may be quite high. One such state might be the metastable $^3\Pi_2$ state.

We have probed this possibility by measuring the photon yield of the $\text{Br-O}_2\text{F-O}_2^*$ reaction. For these measurements, calibrations of the light collection efficiency of our apparatus were made using the well known $\text{O} + \text{NO}$ reaction as a chemical actinometer. For this system, the absolute rate constant for production of photons is known from the work of Fontijn and co-workers (Ref. 35) (as well as a number of other authors (Ref. 36)). Hence, we may define a parameter α which when multiplied by the measured intensity (counts/time) equals this rate:

$$\alpha I = kf[\text{O}][\text{NO}] \quad (14)$$

Here k is the constant determined by Fontijn, et. al., and f is the fraction of the total NO_2^* spectral output that is monitored. For example, if the monochromator were set at a particular wavelength with a particular bandpass, f would be the fraction of the NO_2^* emission passed by the slit. Since the absolute intensity distribution of the NO_2^* emission is known, f can be calculated easily. In our experiments, emissions were observed from scans over a large wavelength region. This procedure is the same, however, as collecting light through a bandpass equal to the region scanned for a time

equal to that necessary to scan one actual bandpass. Hence, equation (14) can still be applied.

For the measurement of α , the concentrations of O and NO were determined using calibrated mass flowmeters and standard titration techniques (Ref. 37). NO₂ photons were counted for scans from 450 nm to 850 nm (the wavelength region of the BrF flame), at 50 nm/minute with 250 μ m slits. Since in this case the bandpass is ~ 0.8 nm, this is the same as counting for 0.96 seconds with a 400 nm bandpass. Determinations of α were made for different O and NO concentrations, yielding an average value $\alpha = 1.0 \pm 0.1 \times 10^7$ photons cm⁻³sec⁻¹ \div counts sec⁻¹.

The BrF B \rightarrow X flame was generated as described above and the intensity scanned for conditions identical to those employed in the NO₂ calibrations. The absolute flowrate of the Br₂/Ar mixture was measured using a calibrated mass flowmeter. The partial pressure of O₂F generated in the cell was known from absorption measurements, and the flowrates of Br₂ used were such that O₂F was in large excess. The measured photon yield (ϕ) is defined as the ratio of the rate of production of photons by the reaction to the flowrate of the limiting reagent (in this case, bromine atoms). Hence,

$$\phi = \frac{\alpha \int_v I(v) dv}{F} \quad (15)$$

where F is the bromine atom flowrate and the integral represents the intensity integrated over the flame volume. The value of the integral was estimated from the measured intensity and the shape and time duration of the flame.

The results of the measurements are presented in Figure 6 as a plot of ϕ vs the bromine atom flowrate. We have assumed that the atom flowrate is twice that of Br_2 , i.e., that all the Br_2 is dissociated by reactions (10) and (11). The data show that the yield decreases with increasing bromine flow. This result agrees with the quenching behavior observed in our experiments and in Reference 34. The limiting photon yield (extrapolated to zero bromine flow) is $\sim 2 \times 10^{-3}$. We note that this is probably an underestimation of the true yield given the assumptions that all the Br_2 is dissociated (and remains so) and all Br atoms are removed only by O_2F .

These results suggest that the $\text{Br-O}_2\text{F-O}_2^*$ system is probably not a viable laser candidate. The 0.2% photon yield suggests that the system is not strongly constrained to form electronically excited states, in qualitative agreement with the suggestion that the initial reaction ($\text{Br} + \text{O}_2\text{F}$) produces vibrationally excited ground state molecules. In this case a broad range of vibrational states would probably be formed, only a small percentage of which would have sufficient energy to be pumped to the B state by collisions with O_2^* .

It is difficult to explain the production of $\text{BrF B}(^3\Pi_0^+)$ by the reaction of molecular bromine with O_2F . It is possible that the dim flame observed results from reaction between Br_2 and F_2 produced by the decay of O_2F . $\text{BrF B} \rightarrow \text{X}$ emission has been observed from flames of Br_2 burning in F_2 (Ref. 38). Our

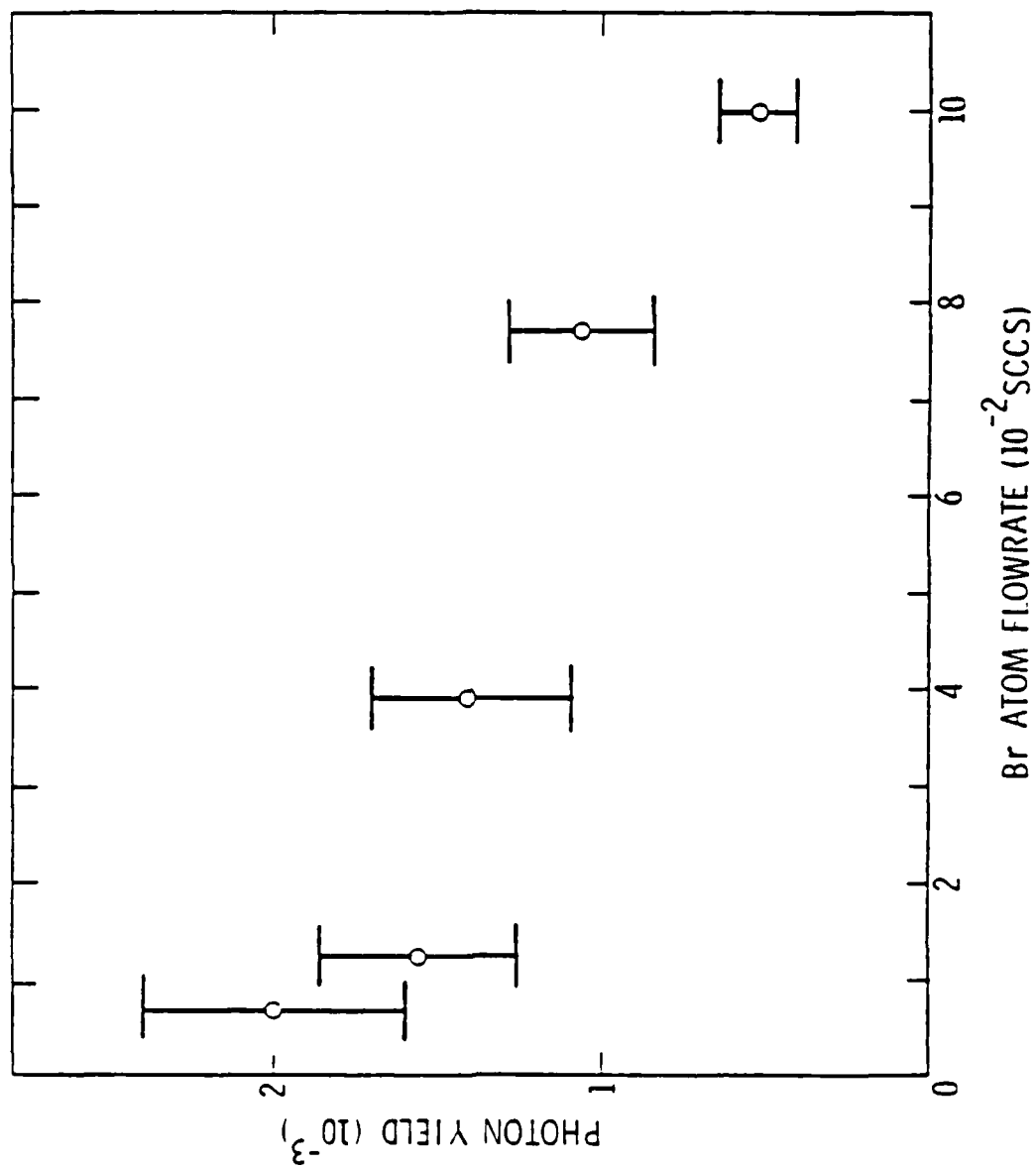
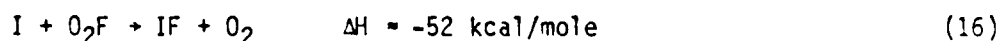


Figure 6. $\text{BrF Br}(^3\Pi_0^+) \rightarrow \text{X}(^1\Sigma^+)$ photon yield vs. Br atom flowrate for the $\text{Br} + \text{O}_2\text{F}_2 \rightarrow \text{BrF} + \text{O}_2 + \text{F}_2$ reaction.

observations of analogous reactions producing excited IF offer some further insight regarding this point (see below).

2. Reactions Producing Excited IF

Lasers based on electronic transitions in IF would have inherently higher gains than those based on BrF, since the transition probabilities for the IF $A \rightarrow X$ and $B \rightarrow X$ transitions should be significantly greater than those for BrF. In addition, the density of rotational and vibrational states is lower for IF. IF is particularly interesting with regard to O_2F reactions since the $A(^3\Pi_1)$ state can be produced directly by the $I + O_2F$ reaction:



The energy of the $A(^3\Pi_1)$ state (48 kcal above the ground state) has been well established in this case by the chemiluminescence experiments of Birks, et al. (Ref. 2). Clyne and co-workers have suggested that IF $A(^3\Pi_1)$ molecules formed by atom recombination may be pumped to the B state by singlet molecular oxygen (among other possible explanations for their results) (Ref. 25). The pumping mechanism of the $I-O_2F-O_2^*$ reaction may therefore be fundamentally different from the mechanism of the analogous bromine reaction, possibly resulting in a higher photon yield for the $B \rightarrow X$ transition.

ICl₂ was chosen as the source of iodine atoms for our initial experiments on the $I + O_2F$ reaction. The apparatus used and the procedures followed were similar to those employed in the BrF experiments. The ICl₂ (PCR) was

purified by degassing at 77K followed by distillation into a trap at 196K. As with Br_2 , a mixture with argon was prepared in a 35L vessel (3% ICl_2). The ICl_2/Ar mixture was added to a stream of microwaved oxygen such that I and Cl atoms were both produced (Ref. 25, 39). Hence the reaction mixture included I, Cl, O_2^* , O_2F and probably $\text{I}^*(5^2\text{P}_{1/2})$ produced by resonant energy transfer from $\text{O}_2^*(^1\Delta_g)$ (Ref. 40). The reaction produced a yellow-green flame consisting primarily of IF B \rightarrow X transitions, with a broadband peak intensity about an order of magnitude less than that obtainable from the BrF system. The weakness of the flame suggested that only a small fraction of the iodine atoms actually reached the reaction zone. Iodine atoms are known to recombine rapidly on surfaces (Ref. 41), and reactions producing iodine oxides have been observed to generate solid wall coatings (Ref. 42). In fact, considerable coating of the vessel walls was noted in these experiments. Hence a photon yield was not measured for this flame since the flowrate of iodine atoms that actually react with O_2F was unknown.

As in the BrF case, the reaction was observed to produce a flame without the assistance of a microwave discharge through O_2 . The flame produced by mixing molecular ICl_2 with O_2F was considerably weaker (perhaps by an order of magnitude) than the emission described above but it was still easily visible and many times more intense than its $\text{Br}_2 + \text{O}_2\text{F}$ counterpart. As in the Br_2 case, such emission might be produced by an $\text{ICl}_2\text{-F}_2$ interaction (F_2 being generated by the decay of O_2F) analogous to the well known $\text{I}_2 - \text{F}_2$ flame. This hypothesis was disproven, however, by an experiment in which O_2F was replaced by a stream of $\text{F}_2:\text{N}_2 = 1:1$. For ICl_2 pressures comparable to those used in the

O_2F experiments, the F_2 partial pressure was varied between 10 and 65 mtorr. A very dim flame resulted, with an intensity no greater than 2% of that produced by $ICl + O_2F$. Hence the $ICl - O_2F$ flame is in fact due to interactions between these two species.

Similar results were obtained from reactions of O_2F with I_2 and HI . A stream of gaseous I_2 was obtained from a saturator in which N_2 (Airco, 99.999%) was passed through a bed of solid I_2 (Malinckrodt). The pressure in the saturator was held at ~92 torr. Hence, at the normal ambient temperature (293K) the stream contained ~0.3% I_2 . HI (Matheson) was purified by fractional condensation at 273K and 77K. A mixture in argon ($HI \approx 12\%$) was prepared in a 3L vessel. The reaction of I_2 with O_2F produced a flame whose intensity was approximately eight times greater than that produced by an equivalent amount of ICl . The peak intensity of the $HI + O_2F$ flame was comparable to that produced by $I_2 + O_2F$. The flame duration was short ($\tau < 5$ msec) in each case, again indicating production rates greater than $10^{11} \text{ cm}^3 \text{ mole}^{-1} \text{ sec}^{-1}$. For the ICl and I_2 systems, comparisons were made with the analogous flames produced by reactions with F_2 . The $ICl-F_2$ flame was very weak as noted above. The $I_2 - F_2$ flame was brighter and extended through the entire body of the cell, having the visual appearance of a recombination reaction. The $I_2 - O_2F$ flame was approximately ten times more intense in the observation zone than was the $I_2 - F_2$ flame at comparable pressures. These findings indicate that the rates of production of excited species by the O_2F reactions are much more rapid than in the F_2 analogues.

Spectra of the emissions produced by the reactions of O_2F with the three iodides were recorded as described above. Each of the systems was observed to yield virtually the same emission spectrum, consisting of a combination of $A(^3\Pi_1) \rightarrow X(^1\Sigma^+)$ and $B(^3\Pi_0^+) \rightarrow X(^1\Sigma^+)$ transitions in IF. Although the relative proportions of $A \rightarrow X$ and $B \rightarrow X$ emissions varied somewhat between the different reactions, the bands present and their relative intensities were unchanged. This result suggests that excited IF is produced by some process common to all three systems. Normally the most intense $A \rightarrow X$ bands were about half the strength of the $B \rightarrow X$ features. A portion of the spectrum showing bands of both transitions is shown in Figure 7. In view of the probable difference between the radiative lifetimes of the two states (the A state should have a longer lifetime by perhaps as much as two orders of magnitude (Ref. 2)), it would seem that the large majority of the electronically excited IF is produced in the $A(^3\Pi_1)$ state. Emission from this state has been reported only once, from the experiments of Birks, et. al., on the $I_2 - F_2$ flame at low pressure (Ref. 2). Our spectrum of the $I_2 - O_2F$ reaction contained most of the $A \rightarrow X$ bands observed by Birks and nine additional bands which have not been previously reported. The frequencies of bands observed in our experiments are presented in the form of a Deslandres table shown in Table III. The data were fitted directly using a multiple regression analysis as described in Reference 22, yielding the following values for the constants of the $A(^3\Pi_1)$ state: $\nu_e = 15696 \pm 6 \text{ cm}^{-1}$, $\omega_e = 378.6 \pm 2.6 \text{ cm}^{-1}$, $\omega_e x_e = 3.4 \pm 0.6 \text{ cm}^{-1}$, $\omega_e y_e = -0.02 \pm 0.03 \text{ cm}^{-1}$. These values are in reasonable agreement with those calculated in Reference 2.

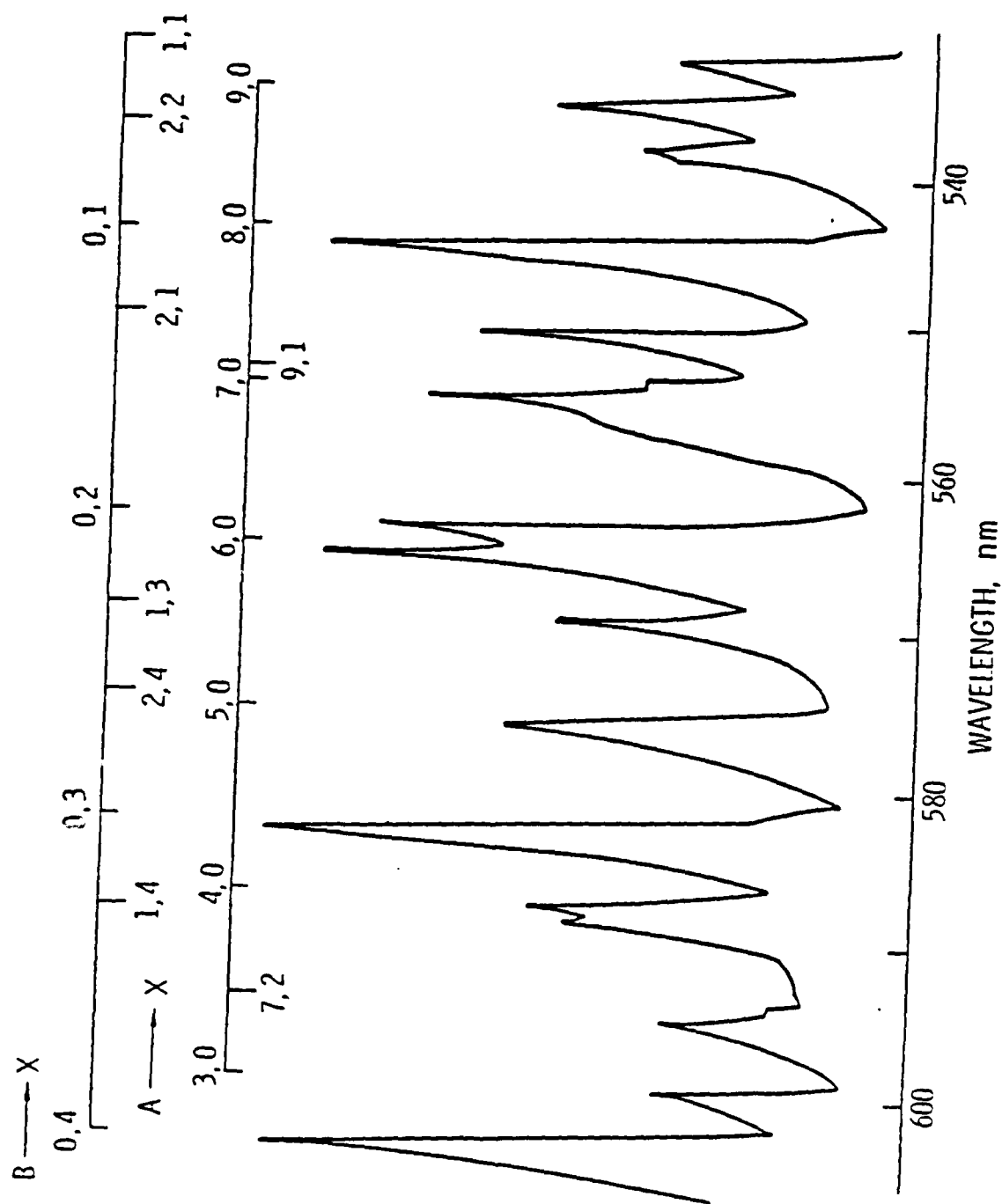


Figure 7. A portion of the emission spectrum obtained from the I_2+O_2F reaction showing bands of both the $B(1/2^+) \rightarrow X(1/2^+)$ and $A(3/2^+) \rightarrow X(1/2^+)$ transitions.

TABLE III

DESLANDRES TABLE FOR IF $A(^3\Pi_1) \rightarrow X(^1\Sigma^+)^a$

v, v''	0	1	2	3
0	[15582] (603)	14979 \pm 3 (597) (371)	14382 \pm 2 (370)	
1	b	15350 \pm 5 (598) (364)	14752 \pm 4	
2	16317 \pm 6 (603) (356)	15714 \pm 5 (364)		
3	16673 \pm 3 (595) (352)	16078 \pm 3 (348)		14881 \pm 6
4	17025 \pm 3 (599) (346)	16426 \pm 6		
5	17371 \pm 3 (336)		16167 \pm 3 (585) (336)	[15582]
6	17707 \pm 3 (326)		16503 \pm 7 (333)	
7	18033 \pm 6		16836 \pm 6	
8	b	b		
9	18666 \pm 4 (604) (304)	18062 \pm 3		
10	18970 \pm 4 (300)	b		
11	19270 \pm 8			

a. Frequencies reported in vacuum wavenumbers.

b. Obscured by $B(^3\Pi_0^+) \rightarrow X(^1\Sigma^+)$ bands.

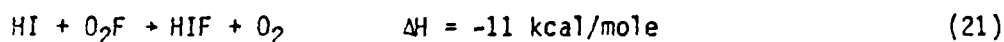
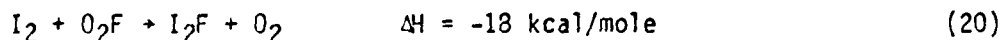
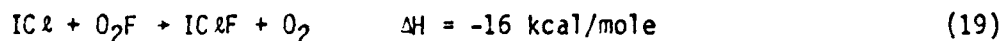
Photon yields were measured as described above for the reactions of O_2F with I_2 and HI . The yields for these reactions were found to be more than an order of magnitude lower than for the $Br-O_2F-O_2^*$ system for comparable limiting flowrates. In both cases the yields exhibited a very strong dependence on the iodide flowrate, indicating quenching by these species or by a reaction product. The yields rose so rapidly with decreasing reagent flowrates that it proved impossible to define a zero pressure limit with any certainty. The data suggested that this limit could be as high as $\phi = 10^{-3}$, however. This behavior is consistent with generation of the $A(^3\Pi_1)$ state as the primary excited emitter in these reactions. The longer radiative lifetime of this state should make it much more susceptible to quenching than the $B(^3\Pi_0^+)$ state.

The reactions of O_2F with ICl , I_2 , and HI can be understood to some extent by consideration of the mechanism currently accepted for the $I_2 - F_2$ reaction. This reaction is thought to proceed as follows: (Ref. 43, Ref. 31).



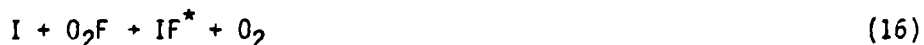
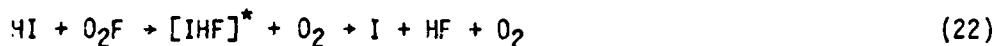
The stable I_2F intermediate has been observed in molecular beam studies of the reaction by Coggiola and co-workers (Ref. 43). Similar triatomic complexes were found for the reactions of F_2 with ICl and HI . In all three cases, formation of the complex is substantially endothermic and hence should be slow (limiting the rate of production of excited IF). The analogous processes

involving O_2F are all exothermic:



Hence these reactions may be expected to be much more rapid than their F_2 counterparts, in accord with the results of our experiments.

Although the formation of triatomic complexes by the $RI + O_2F$ reactions is consistent with the rapidity of these processes, subsequent reaction of any of the three complexes with O_2F (analogous to reaction 18 above) is not sufficiently energetic to produce the excited states of IF observed in our experiments. The reaction of O_2F with the $IClF$ complex should not liberate enough energy to populate even the lowest levels of the $A(^3\Pi_1)$ state of IF. Excited IF could be produced by a reaction of the complexes with fluorine atoms as in reaction (18), but the existence of free fluorine atoms in our system is unlikely given the large excess of O_2F and other scavengers. Also, we noted above that the three reactions produced essentially the same emission spectrum, suggesting a common pumping step. These observations are consistent with a mechanism in which the complexes formed by reactions with O_2F are produced with sufficient energy for dissociation into a diatomic and a free iodine atom. The iodine atom thus produced might then react with O_2F to form excited IF. For example,



The existence of channels analogous to process (22) for the $\text{I}_2 - \text{F}_2$ reaction were reported in the molecular beam study (Ref. 43), and the authors indicated that these channels open at energies only slightly greater than that required for formation of the complex. Given the substantial exothermicities of reactions (19), (20), and (21), it seems plausible that such processes participate in the O_2F reactions. We note, however, that decay of the IClF complex to $\text{I} + \text{ClF}$ is endothermic by ~ 4 kcal/mole. In this case the complex may also decay to $\text{Cl}_2 + \text{IF}$ with an exothermicity of ~ 2 kcal/mole. Chlorine atoms thus produced might react with ICl to generate free iodine atoms or they may be scavenged by excess O_2F . The existence of these other channels may account for the reduced intensity of the $\text{ICl} + \text{O}_2\text{F}$ flame relative to the I_2 and HI analogues.

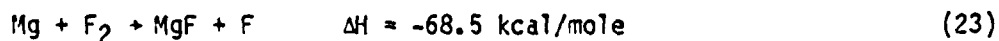
Assuming the bond strength of O_2F to be about 15 kcal/mole (Ref. 13, 14) process (16) liberates ~ 52 kcal/mole. This is sufficient for population of the $\text{A}(^3\Pi_1)$ state of IF up to $v' \sim 7$. The observation of emission from higher levels of the A state suggests that either the O_2F bond strength is less than 15 kcal/mole or that the free iodine atom formed in reaction (22) carries with it some of the energy present in the excited complex. Process (16) might populate the A state directly or it might populate high vibrational levels of the ground state from which the A state may be produced by resonant interactions. The latter process seems more likely in view of the small photon yields measured and

by comparison to the BrF and ClF systems. In these cases, the $A(^3\Pi_1)$ state cannot be produced by the reactions analogous to process (16), yet strong $B \rightarrow X$ emission is still seen when the reactions proceed in the presence of singlet oxygen. We note that the mechanism discussed above (Reactions 22 and 16) may also apply to the $\text{Br}_2 + \text{O}_2\text{F}$ reaction. In this case, however, very little emission is seen since the BrF A state cannot be produced by the second step and no O_2^* is present to generate the B state. The weak $B \rightarrow X$ emission observed may be the result of energy pooling processes between vibrationally excited BrF molecules.

3. O_2F Reactions with $\text{Mg}(^1\text{S})$ and $\text{Mg}^*(^3\text{P})$

Reactions of magnesium atoms with numerous oxidizers have been widely studied, primarily owing to the volatility of this metal at temperatures of a few hundred degrees centigrade. Magnesium reactions are also of interest because the lowest lying metastable excited state of this atom ($\text{Mg}^* ^3\text{P}$, $E = 63$ kcal/mole) can be produced chemically (Ref. 44).

The reaction of magnesium with F_2 has been studied by Eckstrom and co-workers (Ref. 45) using standard chemiluminescence techniques and more recently by Engelke (Ref. 46) using a crossed beam apparatus. The reaction to form MgF liberates 68.5 kcal/mole:



This exothermicity is insufficient for population of the lowest lying state in the excited doublet manifold, the $A(^2\Pi)$ state lying at ~ 79.5 kcal/mole. Eckstrom, et. al., measured the photon yield for the production of this state by reaction (23) to be $\sim 10^{-4}$, in keeping with the generation of MgF^* by recombination of magnesium with F atoms formed in the reaction (Ref. 45). Under the single collision conditions of the crossed beam experiment, the reaction was observed to produce no $A + X$ emission (Ref. 46). In contrast, the analogous reaction of Mg with O_2F would liberate ~ 90.5 kcal/mole, more than enough for direct population of the $A(^2\Pi)$ state. Hence we might expect a considerable enhancement of the $A + X$ photon yield relative to the $Mg + F_2$ case.

Spectroscopic studies of the Group IIA-halides have indicated that transitions between the ground states and lowest lying excited states of these molecules correspond to promotion of a non-bonding electron in the metal atom to orbitals corresponding to excited states of this atom (Ref. 46). Hence, it might be expected that the reactions of excited metastable Mg atoms with RF species would have enhanced $MgF A + X$ photon yields, and this has been borne out by experiments using F_2 . In the crossed beam experiments noted above, it was found that for the $M^* + F_2$ reaction ($M = Mg, Ca, Sr$ or Ba), the cross-section for formation of excited MF was at least an order of magnitude greater than for formation of the ground state (Ref. 46).

In view of these facts, the objectives of the present experiments were to observe the reactions of O_2F radicals with Mg and Mg^* , to measure the spectrum of the emissions and to determine the photon yields for the states

produced. The experiments required a calibrated source of Mg atoms compatible with the technology developed for the generation of O_2F . The method chosen was the direct evaporation of Mg metal in the presence of a carrier gas. The apparatus constructed for this purpose is shown in Figure 8. It consists basically of a closed quartz tube with a small reservoir at the top which holds the powdered metal (50 mesh Mg powder was used in the experiments). Holes in the wall of the reservoir permit flow of a carrier gas (argon) from the tube into the reservoir. Heat is supplied from a resistively heated coil of tungsten wire as shown. Both commercial coils (R.D. Mathis Co.) and hand-made coils were used. The hand-made coils were thinner and hence required less current. Power was supplied to the coil by either a 20 amp "Variac" or by a 15 amp regulated DC power supply. The "oven" temperature was measured using an iron-constantan thermocouple positioned below the metal reservoir as shown in Figure 8.

The metal generator was designed to fit inside a 1.0" i.d. tube, coupled by a 1.0" by 0.75" "ultra-torr" reducing union. The reaction cell designed to accommodate both the metal oven and O_2F generation from $O_2^+AsF_6^-$ is shown in Figure 9. This arrangement, which was arrived at after some iteration, incorporates two frit assemblies for production of O_2F as shown. The O_2F is admitted to the flow tube just downstream of the Mg oven orifice, with the observation window just downstream of the O_2F inlets. Under vacuum conditions, the heat generated by the Mg oven was found to have only a minor effect on the dissociation of the $O_2^+AsF_6^-$ salt relative to the heat applied directly to the frits.

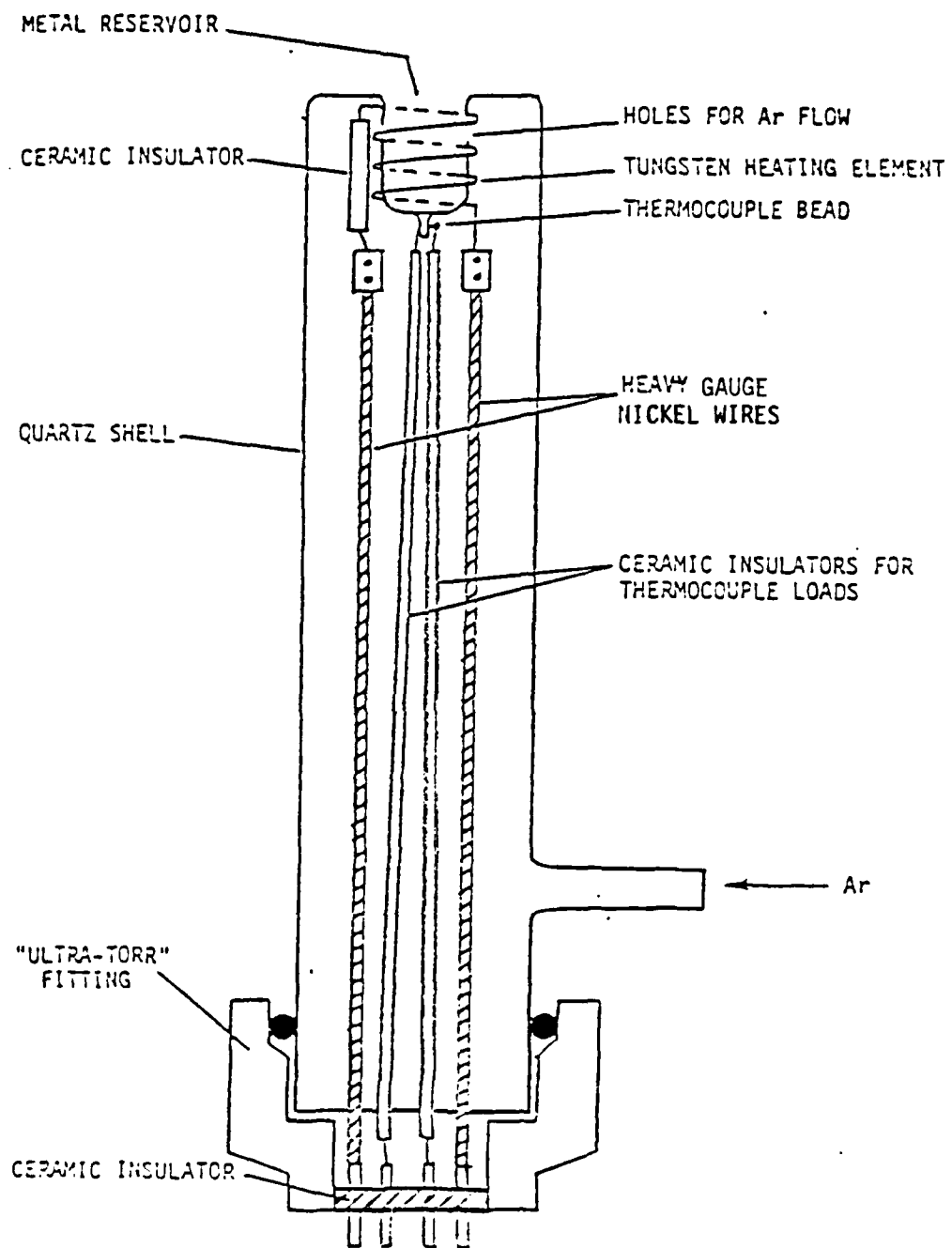


Figure 3. Apparatus used for generation of magnesium vapor.

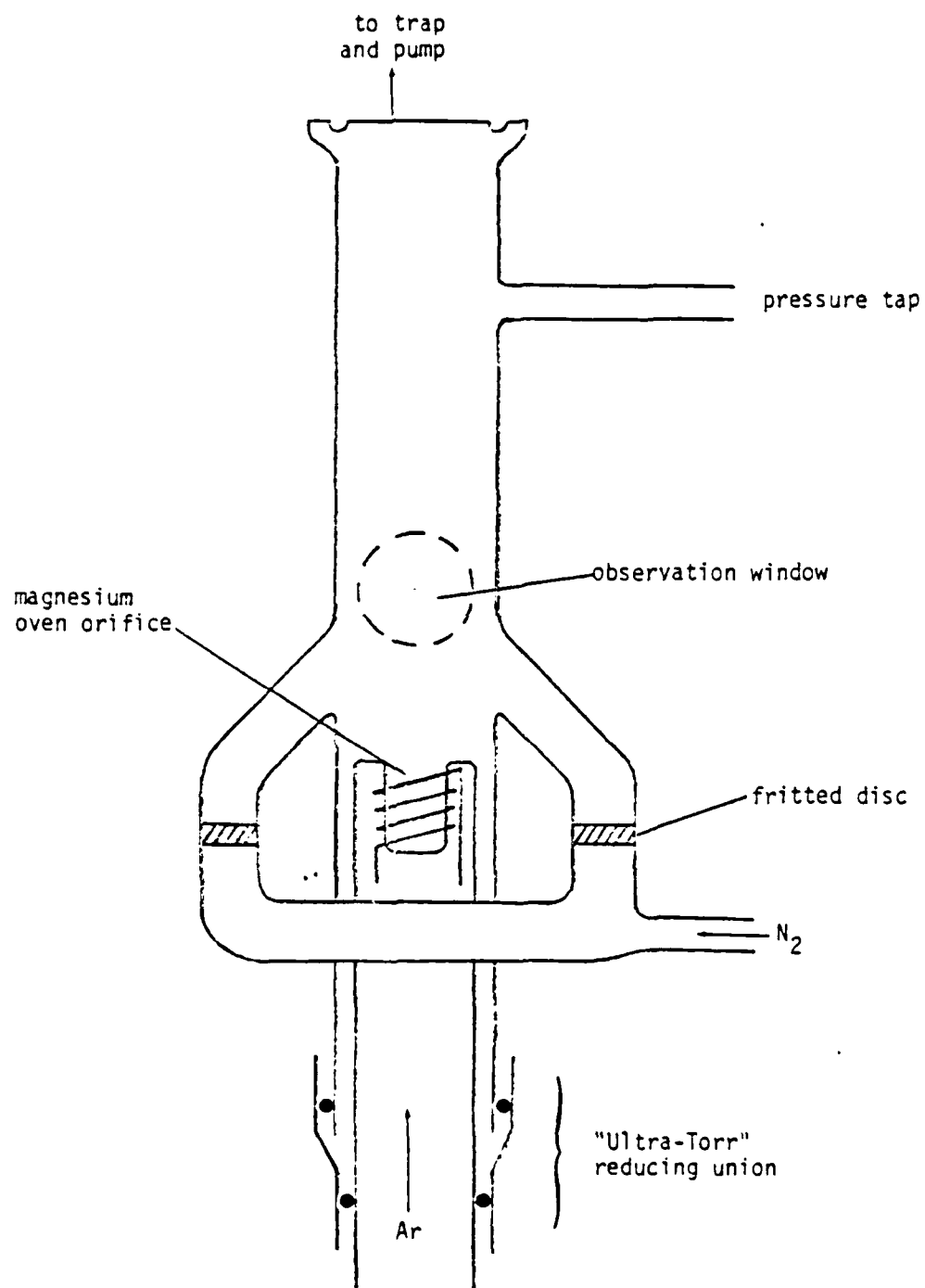


Figure 9. Apparatus used for observation of the reaction of O_2F with magnesium vapor.

In order to measure photon yields for the $\text{Mg} + \text{O}_2\text{F}$ reaction, the flowrate of the metal atoms (the limiting reagent in the system) must be known. Calibrations of the Mg flowrate vs the measured temperature were made by allowing the Mg flow to condense on a removable surface, followed by measurements of the additional weight accumulated on the surface for a given run time. The calibrations were performed using both the cell described above and a separate 1.0" tube used exclusively for this purpose. The surface used for the condensation was an aluminum foil cylinder which lined the inner wall of the tube. The length of the foil liner (extending well above and below the oven orifice) was such that condensation of nearly all the oven effluent was assured. The weight of the foil before and after the runs was measured using a Mettler A30 balance; the minimum weight difference considered to be real was 0.3 mg. The carrier gas used in both the calibrations and the experiments was argon. The argon flowrate was typically 0.67 sccs (sccs = standard $\text{cm}^3 \text{ s}^{-1}$) variations in the argon flowrate by as much as a factor of two were observed to have a relatively minor effect on the Mg flowrate. The calibration run times (up to two hours) were such that a stable equilibrium temperature existed for the major portion of any given run.

Calibration data obtained in this fashion for magnesium are shown in Figure 10. Data are shown for three separate groups of experiments which were separated by a period of months. The calibrations were performed using both homemade and commercial tungsten coils, and both AC and DC power supplies. The agreement between the three groups of runs demonstrates the reproducibility of the Mg flowrates over more than three orders of magnitude. The "gliche"

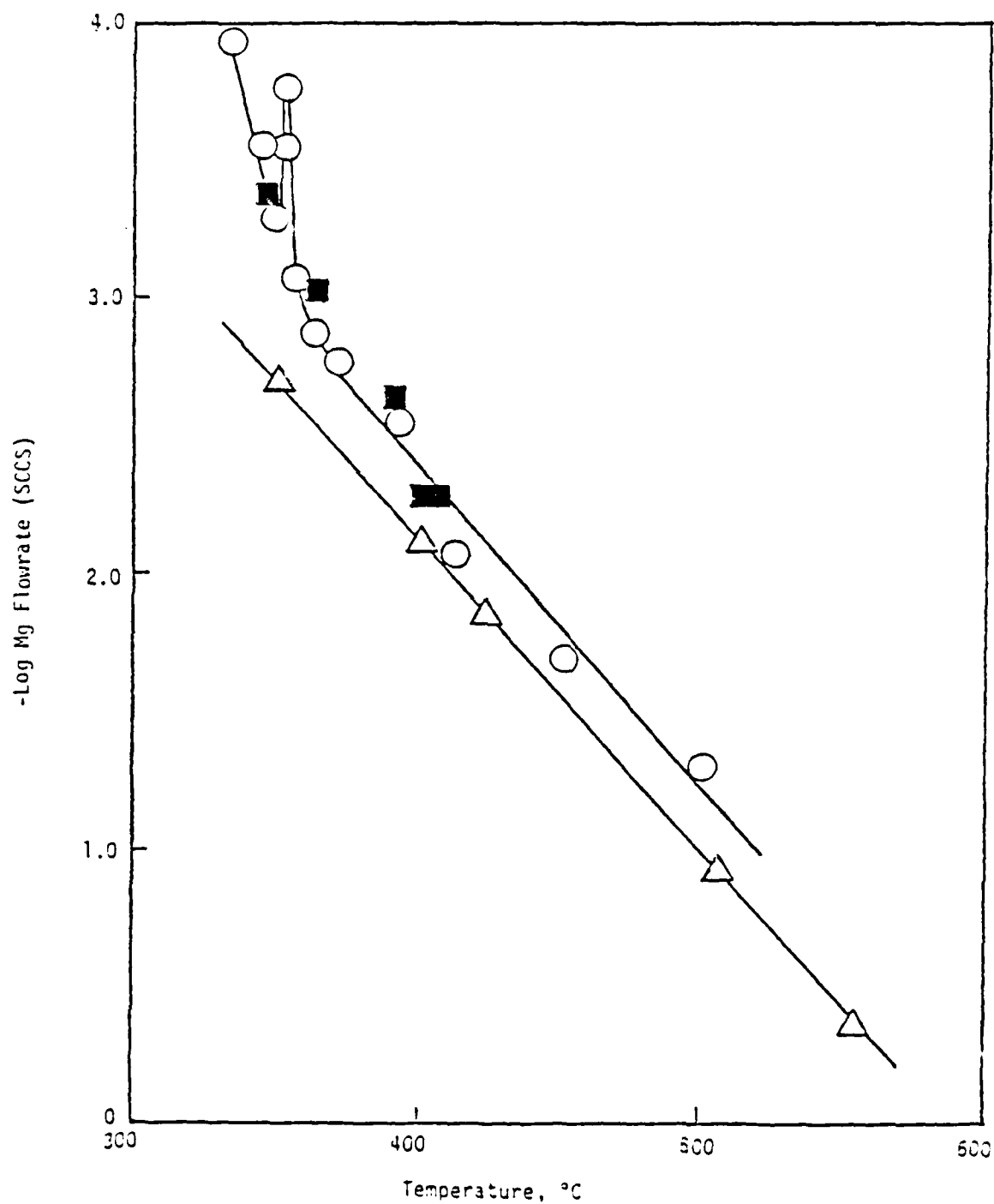


Figure 10. Calibration of the magnesium vapor flowrate vs. temperature measured in the evaporation apparatus (see Figure 8). The triangles, circles, and squares represent data obtained at different times over a period of several months.

shown in the data at $\sim 350^\circ\text{C}$ was quite reproducible and appears to be real. The flowrate data shown, when deconvoluted with the tube area and linear velocity of the flowing gases, yield magnesium densities much greater than the vapor pressures at the temperatures indicated by the thermocouple. Hence the equilibrated temperature in the metal must be higher than in the vicinity of the thermocouple. The temperature recorded thus serves only as a convenient measure of the flowrate.

The results of the initial $\text{Mg} + \text{O}_2\text{F}$ experiments were quite unexpected. The experiments were begun by generating a small (<10 mtorr) concentration of O_2F in the cell with Ar and N_2 carrier gases flowing to give a total pressure of ~ 250 mtorr. Upon application of heat to the magnesium reservoir, a blue flame appeared almost immediately in the mixing zone of the cell. The intensity of the flame increased as the flowrate of Mg increased, becoming quite bright for flowrates as low as 10^{-3} sccs. The flame died out when the $\text{O}_2^+\text{AsF}_6^-$ was consumed or the frit heaters were turned off (in the latter case some emission remained as the heat generated by the Mg oven was sufficient to cause some decomposition by the salt). When the Mg powder was removed from the oven, the intensity of the flame was greatly reduced, although not completely eliminated. It was originally thought that this residual emission was due to magnesium deposits in the oven; later experiments, however, showed the emission to occur even with an apparatus completely uncontaminated with Mg. We attribute the residual emission to an interaction between the "hot" argon passed over the tungsten coils with either of the $\text{O}_2^+\text{AsF}_6^-$ decomposition products (O_2F or AsF_5). In any case, the intensity was

greatly enhanced by the presence of Mg, and can be attributed primarily to an Mg + O₂F interaction.

The full emission spectrum of the flame was recorded using a combination of two gratings (blazed at 300 and 500 nm) in a McPherson model 218 0.3 m monochromator. A GaAs photomultiplier tube and photon counting apparatus were used as in previous experiments. For the UV grating, the response of the entire detection system vs wavelength was calibrated using a deuterium lamp with a known spectral output.

At low Mg flowrates (less than 10^{-4} sccs) and relatively high O₂F concentrations (>10 mtorr), the emission spectrum consists solely of a broad "continuous" emission which is responsible for the blue-white color of the flame. The spectrum of this broadband emission is shown in Figure 11a. Structure could not be resolved within the resolution of our apparatus (~2 nm), although the emission was not smooth and exhibited many irregularities. The emission begins at ~300 nm, reaching a peak at ~370 nm as shown in the figure. The intensity decays gradually with increasing wavelength, and is still quite evident beyond 750 nm. The emission intensity was found to be sensitive to the flowrate of both Mg and O₂F, rising with increased flow of each species; it was much more sensitive to the Mg flow rate, however.

The shoulder shown on the rise of the emission near 310 nm is real, and under some conditions was observed to be a strong banded feature. Further experiments showed that this feature and a portion of the "continuous" emission at longer wavelengths could be attributed to the residual emission noted

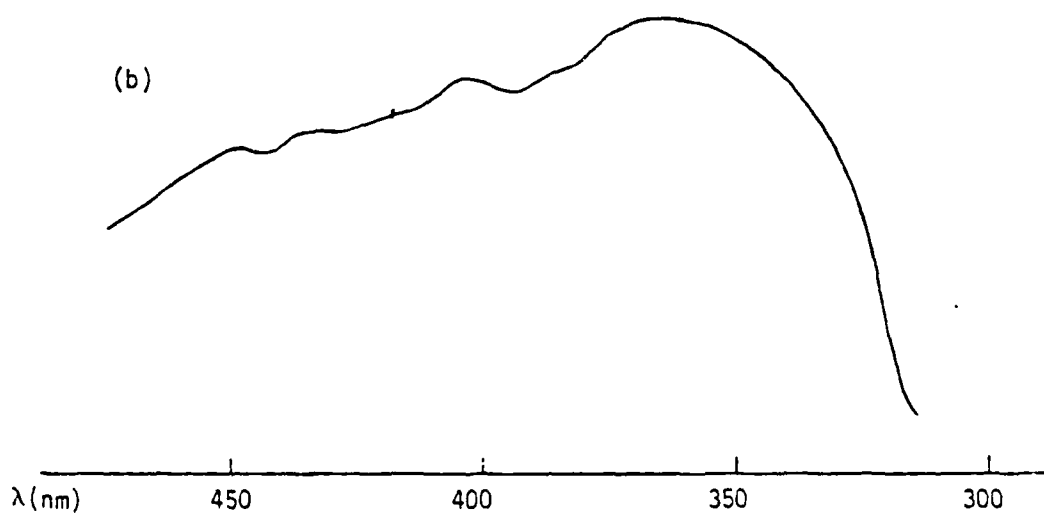
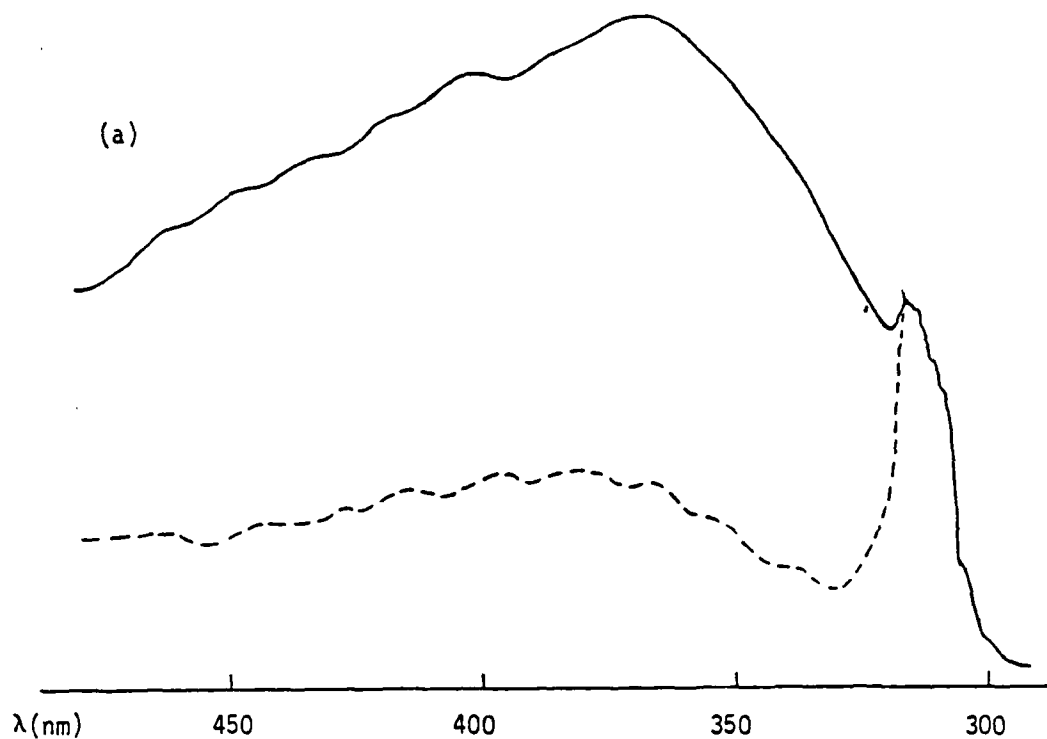


Figure 11. Spectra of broadband emission observed from the $\text{Mg} + \text{O}_2\text{F}$ reaction. (a) total emission (solid line) and contribution from "residual" emission (broken line); (b) "difference" spectrum possibly attributable to excited MgF_2 .

above (thought to be due to interaction between the hot argon and O_2F/AsF_5). The spectrum of this emission, shown as a broken line in Figure 11a, was obtained using a new oven totally uncontaminated with Mg. A number of such comparison spectra were taken at different Mg flowrates in order to firmly identify the portion of the emission caused by the $Mg + O_2F$ reaction. The results of the experiments were all similar to the data shown in Figure 11a. Figure 11b shows the difference between the total and residual emissions, attributable to $Mg + O_2F$.

For relatively low O_2F concentrations (<5 mtorr), a number of new features appeared in the spectrum as the Mg flowrate was increased. Three very intense bands were observed in the vicinity of 360 nm, and these were easily identified as the $\Delta v = 1, 0$, and -1 sequences of the $MgF A(^2\Pi) \rightarrow X(^2\Sigma^+)$ transition. These features are shown in Figure 12. For a fixed O_2F concentration, the intensity of the $A \rightarrow X$ bands increased sharply with increasing Mg flowrate. For a fixed Mg concentration, the $A \rightarrow X$ intensity diminished as the O_2F concentration increased (and the broadband intensity increased). These results suggest that the broadband emission is produced by reaction of O_2F with $MgF^*(A^2\Pi)$, or more likely with its precursor since the short radiative lifetime of the A state (perhaps 10 nsec) would preclude collisions. Such a long lived precursor might be, for example, vibrationally excited MgF ground state molecules which could mix with the A state by resonant interactions. This inference is consistent with production of excited MgF_2 as the "continuum" emitter:

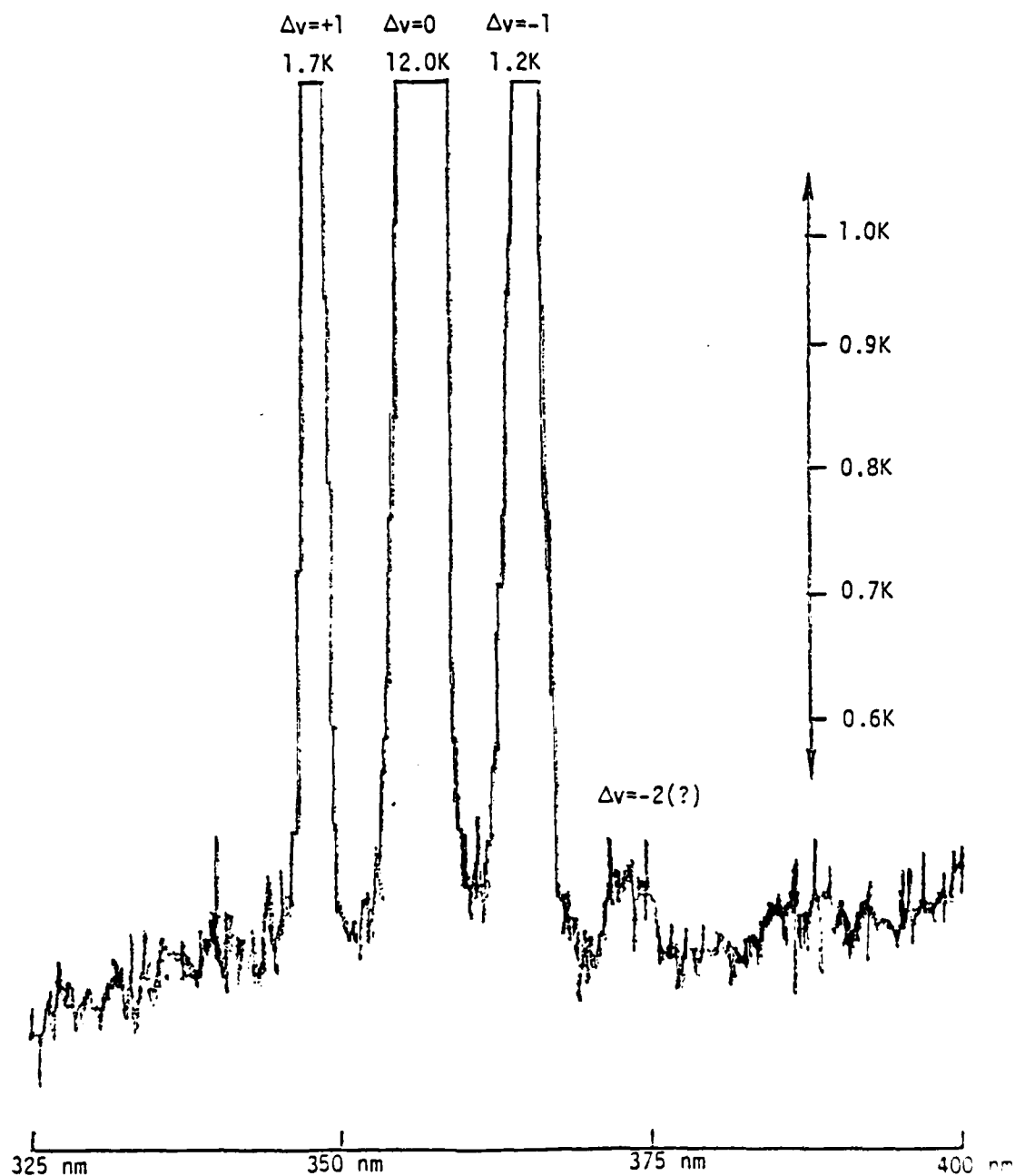
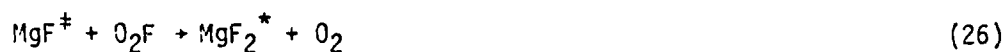


Figure 12. Spectrum showing the $A(2\Pi) \rightarrow X(2\Sigma^+)$ transitions of MgF produced by the $\text{Mg} + \text{O}_2\text{F}$ reaction. Scale to the right indicates intensity.



MgF₂ emission has been previously reported only once, from the recent molecular beam study by Engelke (Ref. 46). The data suggested that the source of the emission in this case was a novel Mg₂ - F₂ four center reaction. The spectrum reported is in fact in fairly good qualitative agreement with that obtained from the present experiments (Fig. 11b).

As the Mg flowrate was increased to still higher values (>10^{-2.5} sccs), emissions from excited states of Mg atoms appeared in the spectrum. The strongest such feature was the Mg* 3S → 3P transition in the vicinity of 518 nm. Considerably less intense emission from the well known 3P → 1S transition at 457.1 nm was also observed, as was 1P → 1S emission at 285.2 nm. Presumably these excited states are pumped by collisional energy transfer from the excited molecular species present in the reaction mixture.

Photon yields for the emissions produced by the Mg + O₂F reaction were measured using the techniques described above. The light collection efficiency of the detection system was calibrated using the O + NO reaction as a chemical actinometer. Several calibrations were performed for scans from 350 to 500 nm at 50 nm/minute, yielding a calibration factor α = 1.5 × 10⁶. This value is in reasonable agreement with those measured previously, given the lower f number of the McPherson monochromator.

Measurements of the yield for the broadband emission were made by scanning from 300 to 500 nm. Hence the assumption was made that the value of α between 300 and 500 nm is essentially the same as from 350 to 500 nm; i.e., that the system has an essentially flat response over this region. Many measurements of the broadband yield were made since the intensity in this case exhibited considerable scatter. The results are shown in Figure 13. The data exhibit a very rapid decline with increasing Mg flowrate, with the limiting yield at zero flowrate being approximately 2%. It should be noted that the data shown were not corrected for the "residual" contribution to the emission discussed earlier. This contribution may be a significant part of the total intensity for the data at lower Mg flowrates, hence clouding the true value of the limiting yield.

The α parameter for the yield of the MgF A + X emission cannot be determined directly since the NO₂ emission is very weak in this region and its intensity distribution is not documented. Hence α in this case was taken to be the value measured for the 350 to 500 nm region, corrected for the different spectral slitwidth used in the measurements, the different scan speed, and the spectral response of the system at 360 nm vs the average over the 350 to 500 nm range. These calculations yielded a value $\alpha = 2.4 \times 10^5$. MgF A + X yields were measured for scans from 340 to 370 nm at 10 nm per minute. The data obtained are shown in Figure 14. The zero flowrate yield in this case is much smaller, on the order of 10^{-5} , but the yield was observed to increase with increasing Mg flowrate as shown. This behavior is in accord with the mechanism postulated above. Increasing the Mg flowrate should

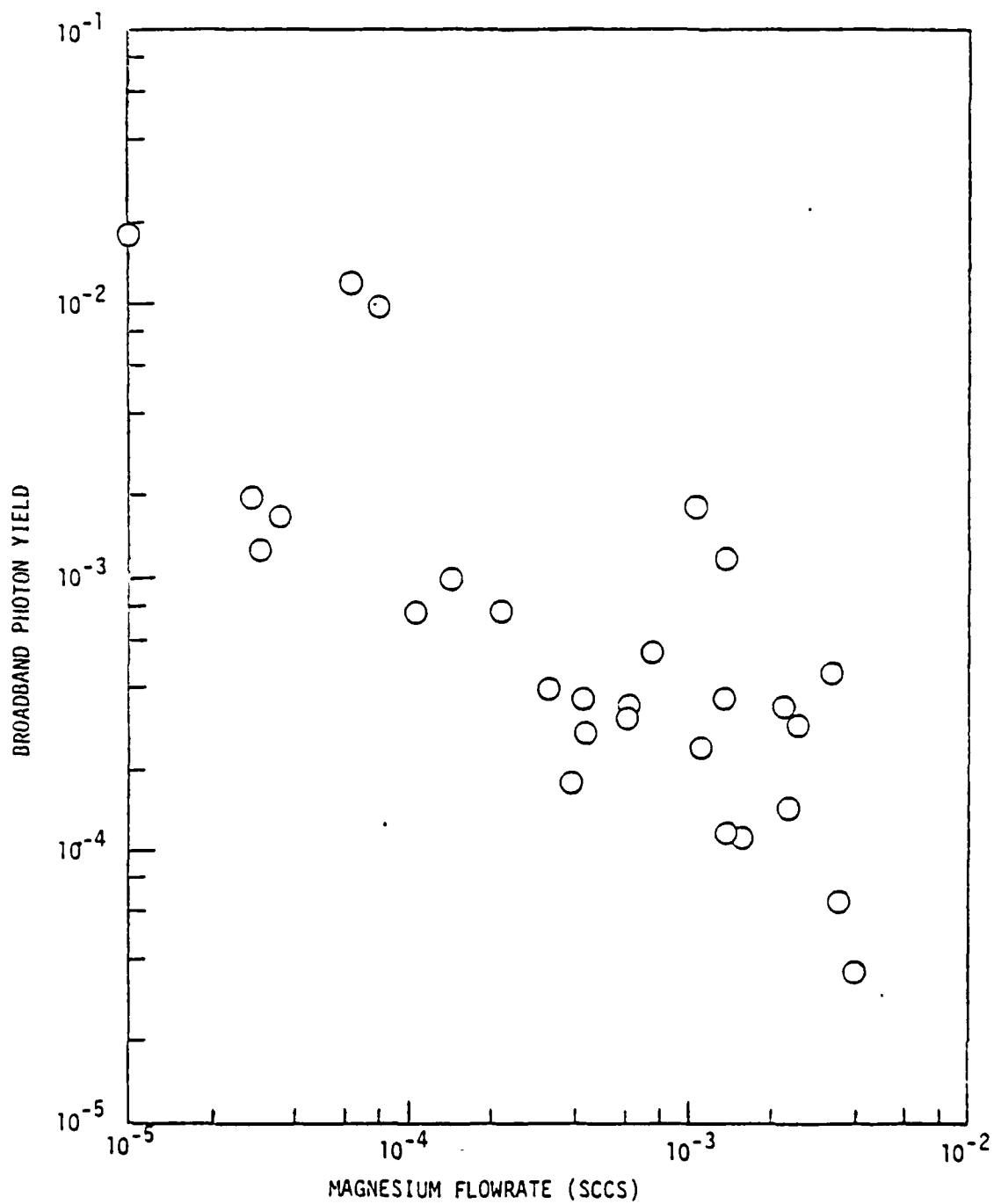


Figure 13. Photon yield of the broadband emission from the $\text{Mg} + \text{O}_2\text{F}$ reaction vs. magnesium flowrate.

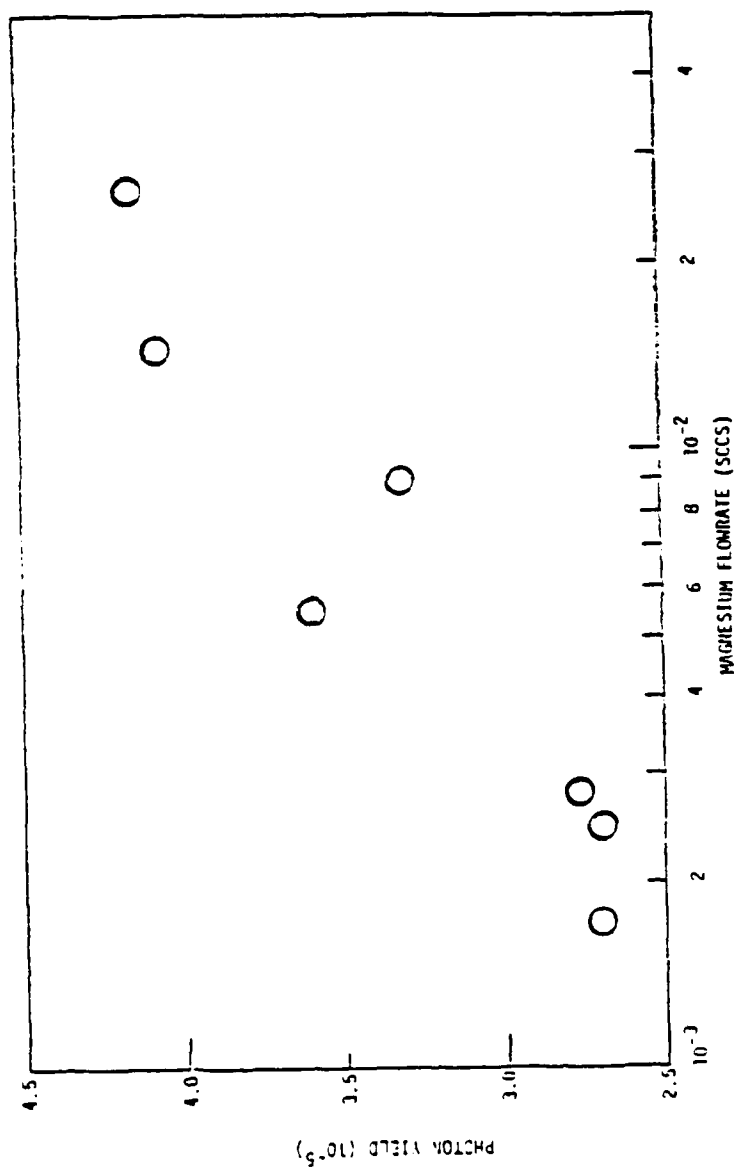


Figure 14. Photon yield of the $\text{MgF } A(2\Pi) \rightarrow X(2\Sigma^+)$ transition vs. magnesium flowrate for the $\text{Mg}+\text{O}_2\text{F}$ reaction.

increase the rate of production of MgF^\pm (Eq. 24) relative to its removal by O_2F (Eq. 26). The steady state concentration of this species (and hence of $\text{MgF}(A^2\Pi)$ by Eq. 25) should therefore increase. Owing to its short radiative lifetime, the $\text{MgF}(A)$ state is not likely to be quenched before radiating. Hence the photon yield also increases.

We note that the measured $A \rightarrow X$ photon yield is even lower than that reported for the $\text{Mg} + \text{F}_2$ reaction, where $\text{MgF}(A)$ can be formed only by recombination (Ref. 45). The fact that the yield for $\text{Mg} + \text{O}_2\text{F}$ is lower supports the hypothesis that free fluorine atoms are not abundant in the system. Apparently, the conversion from MgF^\pm to $\text{MgF}(A)$ (Eq. 25) is not efficient relative to other relaxation or reaction processes. If this conversion is a collision induced process, as suggested by Eq. 25, the $A \rightarrow X$ photon yield should increase with increasing pressure. To test this hypothesis, an experiment was performed in which the intensity of the $A \rightarrow X \Delta v = 0$ sequence was monitored as the total pressure in the system was increased by adding argon. The intensity was observed to rise by 165% for a 26% pressure rise. Although some of this effect may be due to an increase in the linear flow velocity with the pressure rise (i.e., shortening the observation time with respect to the time decay of the $A \rightarrow X$ signal), the result is certainly in accord with the model.

A number of experiments were performed in an attempt to observe the effect of the presence of $\text{Mg}^*(^3\text{P})$ in the system. Mg^* can be produced either chemically (Ref. 44) or by discharge techniques. We chose the latter method since it appeared to be the simplest for our apparatus. Modification of the cell design was required to incorporate the discharge, and two basic

arrangements were used as shown in Figure 15. In both cells, argon was passed through the discharge to produce excited metastable atoms capable of transferring their energy to magnesium. Magnesium vapor was admitted to the Ar/Ar* flow ~10 cm downstream of the discharge for cell a and ~5 cm downstream for cell b. In both cases, addition of Mg to the excited argon produced very bright green luminescence due to $\text{Mg}^* 3\text{S} \rightarrow 3\text{P}$ transitions. For high Mg flowrates the blue $\text{Mg}^* 3\text{P} \rightarrow 1\text{S}$ emission at 457.1 nm could also be seen as a long diffuse tail to the bright green plasma zone.

In the first cell used ("a" in Fig. 15) O_2F was admitted to the flow just downstream from the Mg/Ar* mixing zone (i.e., in the plasma region). Argon was used as the carrier of O_2F in these experiments since N_2 quenched the Ar* metastables. The observation window was just downstream of the O_2F inlet (~3 cm from the oven orifice), and it viewed a portion of the plasma zone. The spectrum recorded for this arrangement included many features attributable to excited Mg and Ar atoms. With no O_2F present, the dominant feature was the $\text{Mg}^* 1\text{P} \rightarrow 1\text{S}$ transition at 285.2 nm. $\text{Mg}^* 3\text{S} \rightarrow 3\text{P}$ and $3\text{P} \rightarrow 1\text{S}$ transitions were also evident, and it was observed that their intensity could be dramatically increased by increasing the Ar flowrate to give a total cell pressure of 800 to 900 mtorr.

The emission spectrum produced by the $\text{Mg}^* + \text{O}_2\text{F}$ interaction was strongly dependent on the O_2F and Mg flowrates. For O_2F pressures less than 5 mtorr and large Mg flowrates, the spectrum consisted of many Mg and Ar atomic transitions, plus some banded features which appeared to be $\text{MgF } A \rightarrow X$ and $B \rightarrow X$ transitions. Positive identification was difficult due to interference

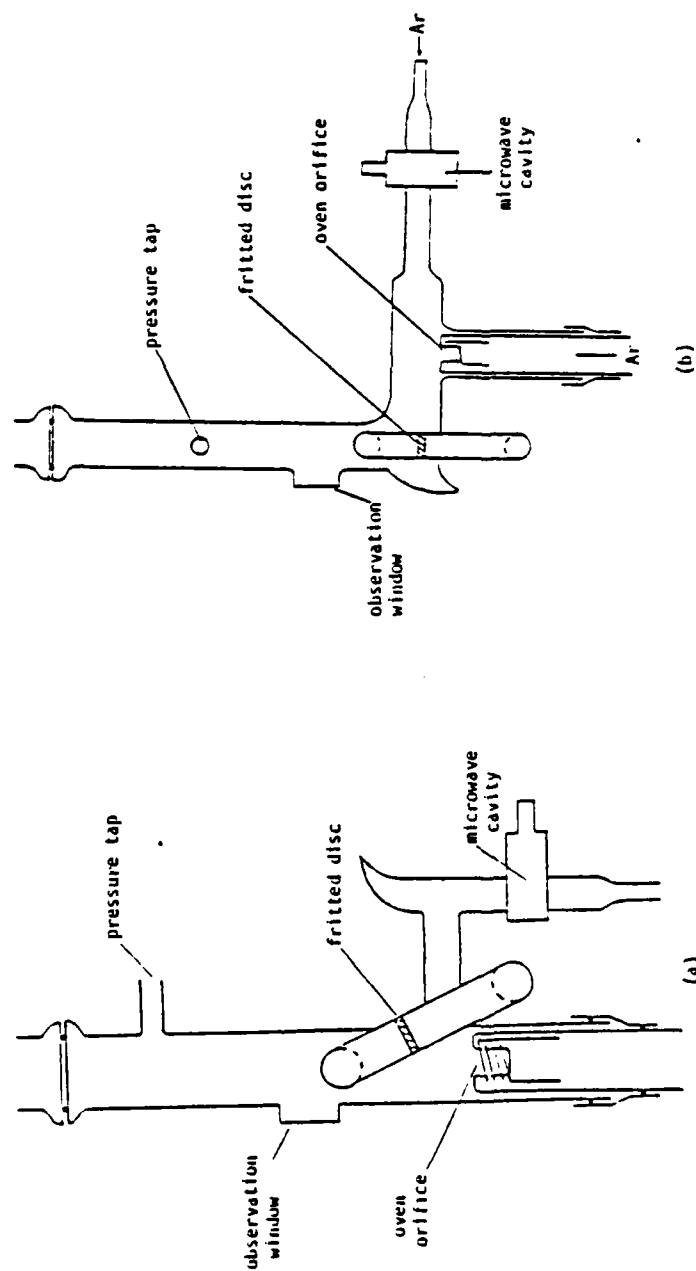


Figure 15. Cells used for observation of the reaction between $\text{Mg}^*(^3\text{P})$ and O_2F_2 .

from the atomic lines. The lines and bands rose from what appeared to be two broad continua, one peaked at ~ 400 nm (apparently the same feature seen in the $\text{Mg(X)} + \text{O}_2\text{F}$ spectrum) and the other peaked near 270 nm. This spectrum is shown in Figure 16a. Increasing the O_2F concentration to partial pressures approaching 10 mtorr almost totally eliminated the green Mg^* emissions. Most of the line and banded features were eliminated from the spectrum, which reduced to the two continua as shown in Figure 16b. It was not possible to determine whether these broadband features increased in intensity with the increase in O_2F pressure. In any case, the $\text{B} \rightarrow \text{X}$ bands and the second (270 nm) continuum are new features which were not present in the $\text{Mg(X)} + \text{O}_2\text{F}$ spectrum. These features may be attributed to the $\text{Mg}^* + \text{O}_2\text{F}$ reaction, or to excitation of MgF or MgF_2 ground state molecules by metastables present in the flow. The $\text{Mg}^*(^3\text{p}) + \text{O}_2\text{F}$ reaction liberates about 153 kcal/mole, sufficient for population of the $\text{MgF A}(^2\pi)$, $\text{B}(^2\Sigma^+)$, and $\text{C}(^2\Sigma^+)$ excited states. No $\text{C} \rightarrow \text{X}$ bands were observed in the spectrum, however.

It was obvious from the experiments that a number of improvements in the spectrum could be realized by moving the observation port well downstream of its present position. Such a change should greatly reduce the interference from short-lived Mg^* and Ar^* atoms created in the plasma, and allow a more definitive characterization of the spectrum and its source. To this end, a new cell was constructed as shown in Figure 15b. The observation window in this cell is approximately 10 cm downstream of the Mg oven, such that it should be looking at only the blue ($\text{Mg}^* 3\text{p} \rightarrow 1\text{s}$) "tail" of the emission from the discharge/mixing zone. The cell worked well in the sense that the emission spectrum in the

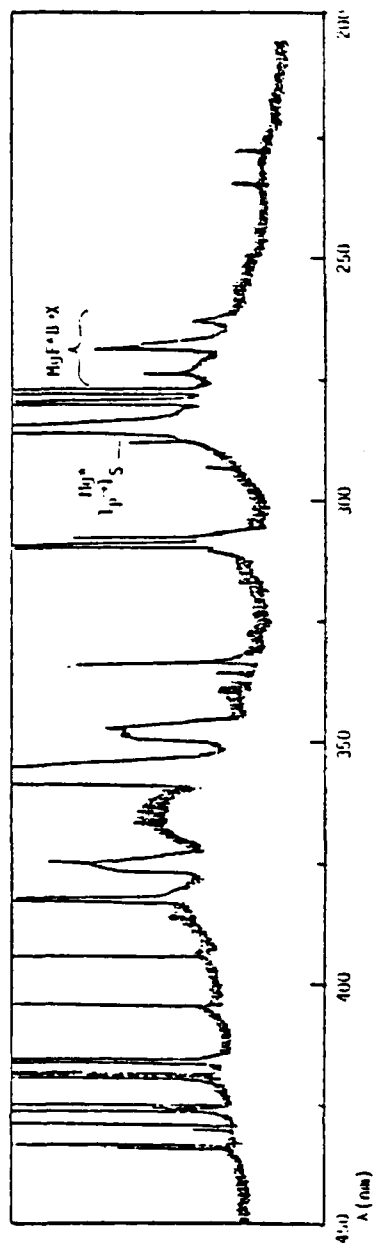


Figure 16a. $\text{Mg}^* + \text{O}_2\text{F}$ emission spectrum for $P_{\text{O}_2\text{F}} < 5$ mtorr.

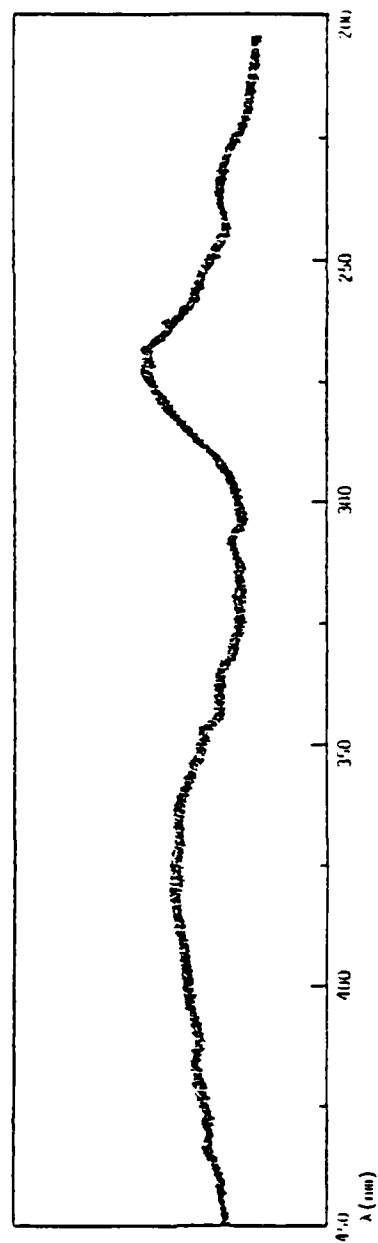


Figure 16b. $\text{Mg}^* + \text{O}_2\text{F}$ emission spectrum for $P_{\text{O}_2\text{F}} \geq 10$ mtorr.

observation zone exhibited only the $\text{Mg}^* (3p + 1s)$ transition at 457.1 nm, with no evidence of excited argon or other Mg states. When O_2F was added to the Mg^* stream just below the window, the spectrum showed the "continuum" ($\lambda > 300$ nm) previously seen from the $\text{Mg} + \text{O}_2\text{F}$ system, but none of the new features found in $\text{Mg}^* + \text{O}_2\text{F}$ experiments in which spectra were taken just downstream of the plasma. Hence we conclude that these features were not caused by the $\text{Mg}^* + \text{O}_2\text{F}$ reaction, but by excitation of species present in the flow by metastables in the plasma.

4. The Reaction of Calcium with O_2F

One would expect the reaction of calcium atoms with O_2F to behave much in the same way the $\text{Mg} + \text{O}_2\text{F}$ reaction does. The dynamics of the two systems should be essentially the same and the arguments noted above concerning the correlation of $\text{Mg} (1s)$ and $\text{Mg}^* (3p)$ with $\text{MgF} (X^2\Sigma^+)$ and $\text{MgF} (A^2\Pi)$, respectively, should hold true for the CaF case. The primary differences lie in the much greater exothermicity of the $\text{Ca} + \text{O}_2\text{F}$ reaction relative to $\text{Mg} + \text{O}_2\text{F}$, and in the fact that the excited electronic states of CaF lie at lower energies. Hence, many more of the excited states of CaF are accessible to the reaction. The $\text{Ca} + \text{O}_2\text{F}$ reaction liberates ~ 113 kcal/mole, sufficient for direct population of the $A(2\Pi)$, $B(2\Sigma^+)$, $C(2\Pi)$, $D(2\Sigma^+)$, $E(2\Sigma^+)$, and $F(2\Pi)$ states of CaF .

The reaction of calcium atoms with molecular fluorine is also highly exothermic and can populate the A, B, C, and D states of CaF . The chemiluminescence produced by this reaction has been studied by Menzinger (Ref. 11) and by Eckstrom and co-workers (Ref. 45). The photon yields measured by Eckstrom,

et.al., are somewhat greater than for MgF; for the CaF case these authors found yields of $\sim 10^{-3}$, 10^{-4} , and 10^{-5} for emissions from the A, B, and C excited states, respectively (Ref. 45). In studies of the reactions of Ca, Sr, and Ba with F_2 , Menzinger noted the production of "continuum" emission in addition to the well known banded features (Ref. 11). The broadband emission was attributed to excited MF_2 molecules, possibly produced by two body recombination ($M + F_2 \rightarrow MF_2^*$) analogous to the mechanism proposed by Jonah and Zare for the $Ba + O_2$ case (Ref. 47).

Hence, on the basis of the energetics of the $Ca + F_2$ and $Ca + O_2F$ systems we would expect little difference between the emissions produced by the two reactions. Higher lying CaF states (D, E, and F) may be produced by the O_2F reaction. Also, broadband CaF_2 emission might be enhanced in the O_2F cases owing to a mechanism analogous to reactions (24) and (26) above.

The techniques used for the generation of calcium vapor and observation of its reaction with O_2F radicals were nearly identical to those described above for the Mg case. A new oven assembly was constructed and calibrations of the Ca flowrate were performed using the weight difference technique. The calibration data are shown in Figure 17. The two points labeled with triangles were obtained using a single large calcium turning in the oven reservoir; the other data were measured using several small turnings. The flowrates measured were somewhat higher for the latter case, possibly attributable to the greater metal surface area. The reproducibility of the measurements was good, as indicated by the plot. The temperatures required were much higher than in the Mg case, as expected, but calcium flowrates comparable to those used in the Mg + O_2F experiments were generated easily.

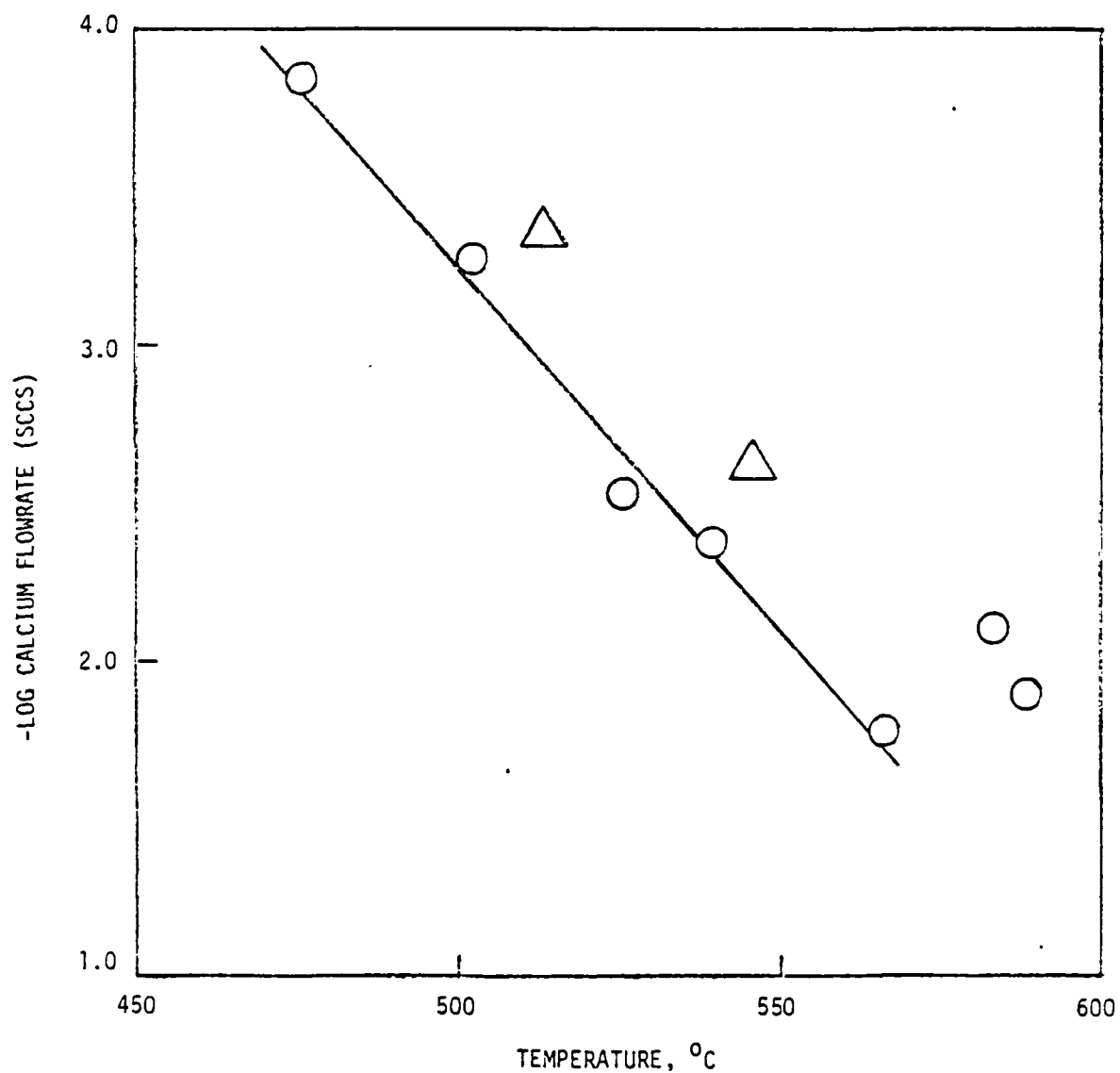


Figure 17. Calibration of the calcium vapor flowrate vs. temperature measured in the evaporation apparatus. The triangles represent data taken using a single large calcium turning; the circles represent data taken using several smaller turnings.

The procedures and apparatus used for the $\text{Ca} + \text{O}_2\text{F}$ experiments were the same as those described above. For a moderate O_2F flowrate, application of current to the oven coils resulted in a blue-white luminescence like that previously observed in the magnesium experiments, apparently due to the "residual" emission noted above. As the oven temperature was increased (still at an extremely low Ca flowrate), the blue flame intensified and appeared to persist throughout the cell and into the pumping line. The color of the flame was not a pure blue as before but seemed to have a yellow-white hue. As the measured oven temperature reached $\sim 540^\circ\text{C}$ (corresponding to a calcium flowrate of $\sim 3 \times 10^{-3}$ sccs) a yellow flame appeared in the reservoir area. The yellow flame became extremely intense with further increases in the calcium flowrate. For a flowrate of $\sim 10^{-2}$ sccs, the intensity of the flame (identified as $\text{A} \rightarrow \text{X}$ CaF emissions) was about ten times the intensity of the analogous MgF $\text{A} \rightarrow \text{X}$ emission for a comparable Mg flowrate.

The spectrum of the $\text{Ca} + \text{O}_2\text{F}$ flame in the visible region was measured using a grating blazed at 500 nm in the McPherson 0.3 m monochromator. The data obtained are shown in Figure 18. The spectrum exhibits the $\Delta v = +1, 0, -1$, and -2 sequences of the CaF $\text{A} \rightarrow \text{X}$ transition, the $\Delta v = 0$ sequence being nearly ten times the strength of any other feature present in the spectrum. The structure at the top of the bands is due to the $^2\Pi_{3/2} - ^2\Pi_{1/2}$ splitting in the A state. The spectrum also exhibits emission from the $\Delta v = +1, 0$, and -1 sequences of the $\text{B}(^2\Sigma^+) \rightarrow \text{X}(^2\Sigma^+)$ transition as shown. In general, the visible portion of the spectrum is nearly identical to that reported for the $\text{Ca} + \text{F}_2$ reaction (Ref. 11).

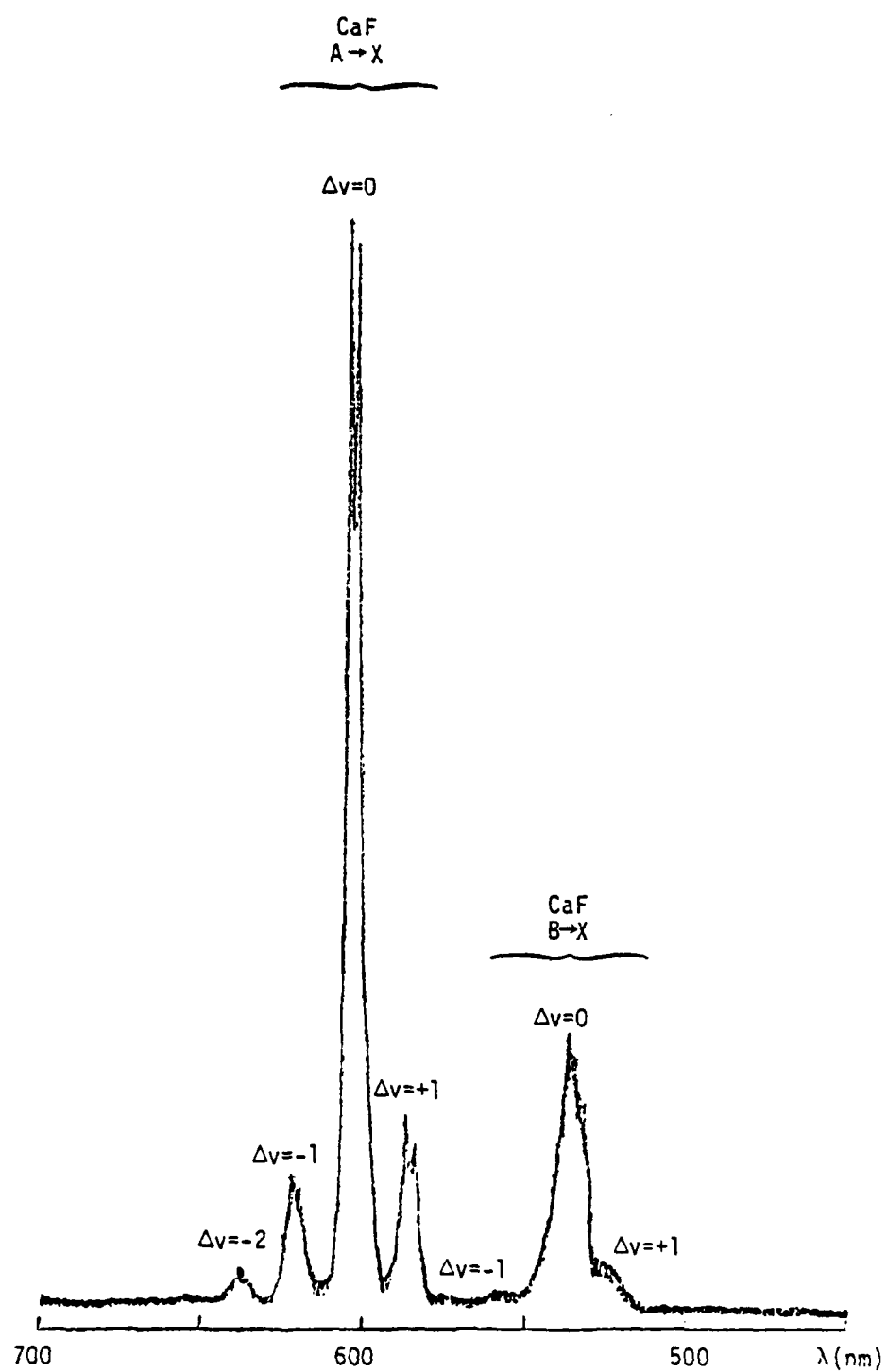


Figure 18. Spectrum obtained in the visible region from the $\text{Ca} + \text{O}_2\text{F}$ reaction, showing the $\text{A}(\text{ }^2\Pi) \rightarrow \text{X}(\text{ }^1\Sigma^+)$ and $\text{B}(\text{ }^1\Sigma^+)$ transitions of CaF .

The spectrum of emission produced by the $\text{Ca} + \text{O}_2\text{F}$ reaction in the ultraviolet region was recorded using a grating blazed at 300 nm in the McPherson monochromator. The spectrum obtained is shown in Figure 19. The dominant features are the sharp banded sequences ($\Delta v = +2, +1, 0, -1, \text{ and } -2$) of the $\text{CaF C} \rightarrow \text{X}$ transition. The intensity of these features was roughly equivalent to that of the $\text{B} \rightarrow \text{X}$ transition shown in Figure 18. The weaker structure at lower wavelengths may be a continuation of the $\text{C} \rightarrow \text{X}$ emission or may possibly be due to $\text{CaF D} \rightarrow \text{X}$ emission; a positive identification was not possible. The $\text{C} \rightarrow \text{X}$ features rest on a strong continuum which appears to rise to a peak in the vicinity of 350 nm. The "pointed" nature of the maximum actually results from the presence of the $\text{C} \rightarrow \text{X } \Delta v = -2$ sequence at this wavelength, which was resolved in a number of spectra.

The sharp band at ~358 nm is not part of the $\text{C} \rightarrow \text{X}$ emission, and in fact does not appear to be due to CaF at all. Reduction of the calcium flowrate to a level just below that required for appearance of the $\text{CaF A} \rightarrow \text{X}$ emission did not appreciably diminish the intensity of this feature. For this reduced calcium flowrate and an increased O_2F flowrate ($P_{\text{O}_2\text{F}} > 10$ mtorr), the spectrum reduced to a continuum emission with the 358 nm feature still present. Small satellite bands were evident on either side of the 358 nm band. In fact, the spectrum obtained for these conditions was almost identical to that produced by the $\text{Mg} + \text{O}_2\text{F}$ reaction, with the bands corresponding to the $\text{MgF A} \rightarrow \text{X}$ transition (see Fig. 12). This result is highly suggestive of a magnesium impurity in the calcium sample. We note that the oven temperatures used in the calcium experiments were much higher than those necessary to produce strong MgF

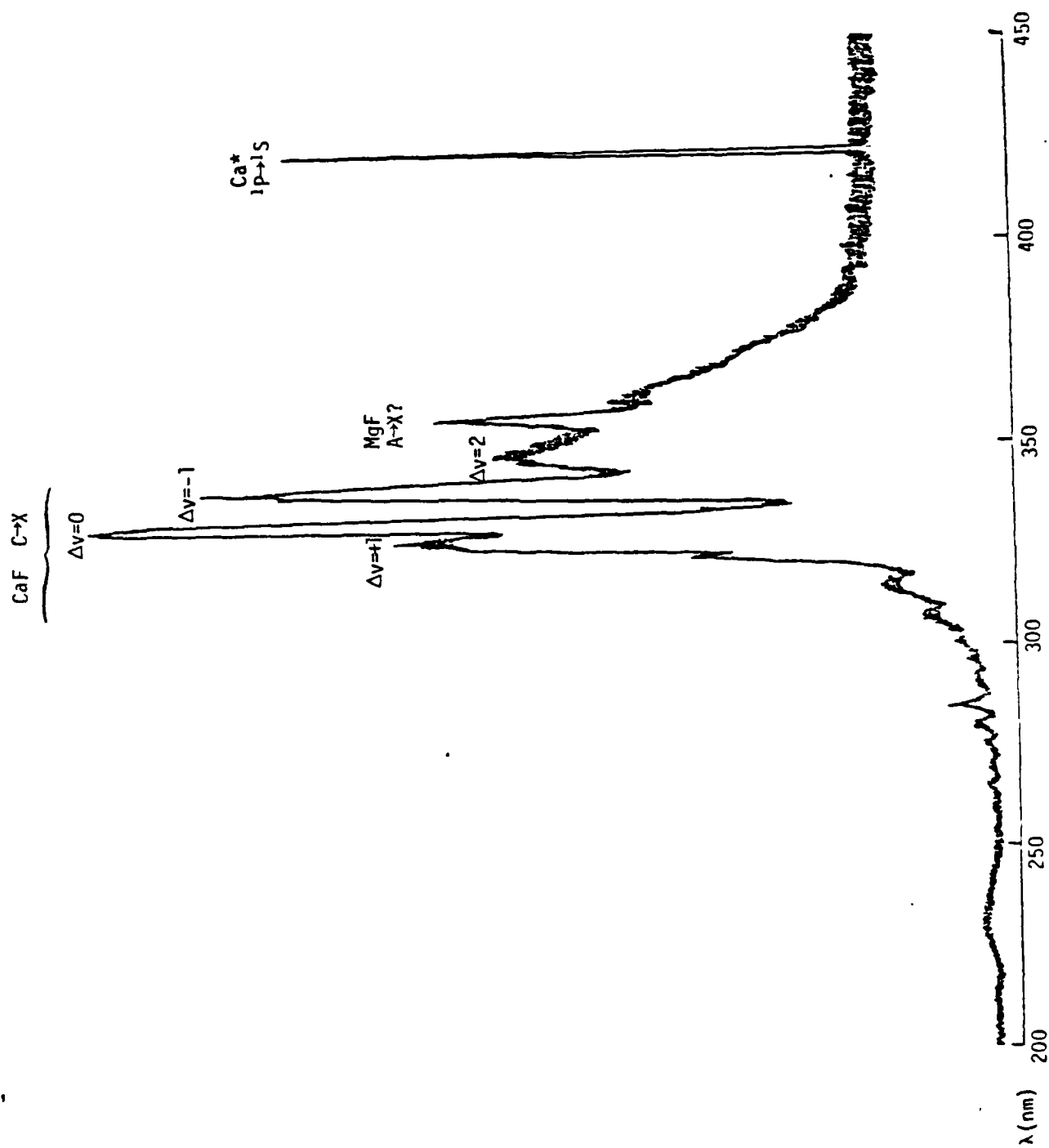


Figure 19. Spectrum of ultraviolet emission obtained from the $\text{Ca} + \text{O}_2\text{F}$ reaction.

emissions in the $\text{Mg} + \text{O}_2\text{F}$ experiments. This possibility has the further result of leaving the source of the continuum emission in the $\text{Ca} + \text{O}_2\text{F}$ experiments in doubt, since it too might be caused by a magnesium impurity.

Additional features present in the $\text{Ca} + \text{O}_2\text{F}$ UV spectrum include the $\text{Ca } ({}^1\text{P} \rightarrow {}^1\text{S})$ atomic line at 422.7 nm and a weak continuum peaking near 230 nm. The atomic line was also reported to appear in the spectrum produced by $\text{Ca} + \text{F}_2$ (Ref. 11), and probably results from energy transfer to calcium atoms from an excited molecular species (e.g., $\text{CaF}^* \text{C}({}^2\Sigma^+)$). The identity or source of the small continuum is unknown; we note, however, that CaF absorption in this region has been reported by Fowler (Ref. 48).

Photon yields were not explicitly measured for the calcium system. It is clear, however, from intensity comparisons at comparable flowrates that the yield of $\text{CaF } \text{A} \rightarrow \text{X}$ emission is about ten times that of $\text{MgF } \text{A} \rightarrow \text{X}$ emission, or on the order of 10^{-4} . Again, this is lower than reported for the $\text{Ca} + \text{F}_2$ reaction. In any case it is clear that the production of electronically excited states is not a major route for this system.

IV. CONCLUSIONS

The results described above have demonstrated the production of a number of electronically excited diatomic fluorides by chemical reactions of O_2F radicals. On the whole, the processes studied are quite different from the analogous reactions involving molecular fluorine. These differences were particularly evident in regard to the nature of the states produced (in some cases inaccessible by direct reactions with F_2) and the rapidity of the processes involved (e.g., the reactions of molecular halides with O_2F). The data obtained consequently yielded new spectroscopic information regarding the $A \rightarrow X$ and $B \rightarrow X$ transitions of BrF and IF (as well as $C\&F$ in previous experiments), and the visible-UV emission from excited MgF_2 .

It is apparent from the measured photon yields, however, that the reactions studied are not strongly constrained to produce electronically excited product molecules. The predominant mechanisms in these reactions would appear to channel the energy liberated into vibrational modes of the products. The visible and UV emissions observed probably stem from mixing of the populated vibrational levels with near resonant levels of the excited electronic states in question, or from V-E collisional energy transfer. The results of both the halogen + O_2F and metal + O_2F experiments suggested mechanisms involving such long-lived precursor states, with the radiating species being produced indirectly.

The fact that in most cases emissions were observed from states near the thermodynamic limit for the energy liberated by the reactions suggests that

a fair proportion of the exothermicity enters product vibrational modes. In order for this to occur, only a small amount of the energy gained by formation of the R-F bond must be channeled into product translation. During the collision the O_2 must not recede from the fluorine during the formation of the R-F bond ("repulsive energy release"(Ref. 49)), but rather it must be relatively uninvolved in the collision until most of the energy has been gained from R-F bond formation ("attractive energy release"(Ref. 49)). This latter case is more like a normal recombination reaction. The results of our experiments in fact reinforce the idea that O_2F reactions are dynamically similar to three body recombinations. Of course the reactions with the metals Mg and Ca are somewhat more complex, since it seems likely that in these cases an electron jump at long range takes place to form the ionic ground states of the MgF and CaF molecules.

Given this scenario, it is clear that the reactions of O_2F with ground state atoms are not viable candidates for chemical laser systems, other than in special cases where ground state reagents may correlate directly with excited products. It would seem more likely that direct production of electronically excited species would result from reactions of O_2F with electronically excited atoms, which normally correlate with excited RF products. A case in point would be the reactions of metastable excited alkaline earth atoms (3P) with O_2F as discussed above. The experiments performed, using a microwave discharge for production of the excited atoms, did not bear out this hypothesis. These results are contradictory to similar studies involving F_2 , and at the present time we consider this issue to be open to further investigation. Experiments

using alternative sources of Mg^* and Ca^* , e.g., chemical methods, should be performed before a final conclusion can be drawn. Similar circumstances apply to the reactions of $\text{I}^*(^2\text{P}_{1/2})$ and $\text{Br}^*(^2\text{P}_{1/2})$ with O_2F , which should correlate with product halogen monofluorides in the $\text{B}(^3\Pi_0^+)$ states.

REFERENCES

1. M.A.A. Clyne and I.S. McDermid, J. Chem. Soc., Faraday Trans. 2, 74, 664 (1978); 1376 (1978).
2. J.W. Birks, S.D. Gabelnick, and H.S. Johnston, J. Mol. Spectrosc., 57, 23 (1975).
3. M.A.A. Clyne, J.A. Coxon, and H.W. Cruse, Chem. Phys. Lett., 6, 57 (1970).
4. R.A. Harris and J.A. Montgomery, Jr., AFWL-TR-73-273, "Laser Digest," 1973.
5. M.J. Bina and S.G. Hadley, AFWL-TR-73-273, "Laser Digest," 1973.
6. R.L. Byer, R.L. Herbst, H. Kildal, and M.D. Levenson, Appl. Phys. Lett., 20, 463 (1972).
7. F.J. Wodarczyk and H.R. Schlossberg., J. Chem. Phys., 67, 4476 (1977).
8. R.D. Coombe and A.T. Pritt, Jr., Chem. Phys. Lett. 58, 606 (1978).
9. J.M. Herbelin and N. Cohen, Chem. Phys. Lett., 20, 605 (1973).
10. J.M. Herbelin, Chem. Phys. Lett., 42, 367 (1976).
11. M. Menzinger, Can. J. Chem., 52, 1688 (1974).
12. J.L. Gole, "Electronic Transition Lasers," Vol. II, L.E. Wilson, S.N. Suchard, and J.I. Steinfeld, Eds., MIT Press, Boston, 1977, p 136.
13. J.B. Levy and B.K. Wesley Copeland, J. Phys. Chem., 69, 408 (1965).

14. T.J. Malone and H.A. McGee, J. Phys. Chem., 69, 4338 (1965).
15. R.W. Fessenden and R.H. Schuler, J. Chem. Phys., 44, 434 (1966).
16. P.N. Noble and G.C. Pimentel, J. Chem. Phys., 44, 3641 (1966).
17. P.P. Chegodaev, V.I. Tupikov, and E.G. Strukov, Russ. J. Phys. Chem., 47, 746 (1973).
18. V.S. Al'zoba, P. P. Chegodaev, and V.I. Tupikov, Dokl. Akad. Nauk. SSSR, 206, 143 (1977).
19. A.R. Young, II, T. Hirata, and S.I. Morrow, J. Amer. Chem. Soc., 86, 20 (1964).
20. J. N. Kieth, I.J. Solomon, I. Sheft, and H.H. Hyman, Inorg. Chem., 7, 230 (1968).
21. R.D. Coombe, A.T. Pritt, Jr., and D. Pilipovich, "Electronic Transition Lasers," Vol. II, L.E. Wilson, S.N. Suchard, and J.I. Steinfeld, Eds., MIT Press, Boston, 1977, p 107.
22. R.D. Coombe, D. Pilipovich, and R.K. Horne, J. Phys. Chem., 82, 2484 (1978).
23. H.J. Schumacher, A. Schmitz, and P.H. Brodersen, Anal. Assoc. Quim. Arg., 38, 98 (1950).
24. W. Stricker and L. Krauss, Z. Naturforsch. A, 23, 1116 (1968).
25. M.A.A. Clyne, J.A. Coxon, and L.W. Townsend, J. Chem. Soc., Faraday Trans. 2, 68, 2134 (1972).

26. P.P. Chegodaev, V.I. Tupikov, E.G. Strukov, and S. Ya. Pshezhetskii, High Energy Chem., 12, 98 (1978).
27. R.A. Durie, Can. J. Phys., 44, 337 (1966).
28. J.A. Coxon and A.H. Curran, J. Photochem., 9, 183 (1978).
29. P.A. Brodersen and J.E. Sicre, Z. Physik, 141, 515 (1955).
30. M.A.A. Clyne, A.H. Curran, and J.A. Coxon, J. Mol. Spectrosc., 63, 43 (1976).
31. M.A.A. Clyne and I.S. McDermid, J. Chem. Soc., Faraday Trans. 2, 72, 2252 (1976).
32. J.A. Coxon, Chem. Phys. Lett. 33, 136 (1975).
33. M.A.A. Clyne and H.W. Cruse, Trans. Faraday Soc., 67, 2869 (1971).
34. M.A.A. Clyne and I.S. McDermid, J. Chem. Soc., Faraday Trans. 2, 73, 1094 (1977).
35. A. Fontijn, C.B. Meyer, and H.I. Schiff, J. Chem. Phys., 40, 64 (1964).
36. See for example G.A. Woolsey, P.H. Lee and W.D. Slafer, J. Chem. Phys., 67, 1220 (1977).
37. M.A.A. Clyne, "Reactions of Atoms and Free Radicals Studied in Discharge Flow Systems," Physical Chemistry of Fast Reactions, Vol. I, B.J. Levitt, Ed., Plenum Press, London, 1973, pp 245-330.
38. R.A. Durie, Proc. Roy. Soc., A207, 388 (1951).

ABBREVIATIONS AND SYMBOLS (CONTINUED)

\dot{N}_H	Molar flux of atomic hydrogen at the nozzle surface
D_{H-M}	Diffusion coefficient for hydrogen atoms in argon within the gaseous plenum
V_5	Mean flow velocity of gas moving toward the nozzle inlet
A^*	Surface area of subsonic portion of nozzle
η_x	Molar flux of species x into reaction zone
θ	A ratio of molar fluxes flowing into the reaction zone

END

DATE
FILMED

8-82

DTIC